Multiphoton multimode polarization entanglement in parametric down-conversion

A. Gatti,[1] R. Zambrini,[2] M. San Miguel,[2] and L. A. Lugiato[1]
[1]*INFM, Dipartimento di Scienze CC FF MM, Universitá dell'Insubria, Via Valleggio 11, 22100 Como, Italy*
[2]*IMEDEA, Campus Universitat Illes Balears, E-07071 Palma de Mallorca, Spain*
(Received 19 June 2003; published 19 November 2003)

We study the quantum properties of the polarization of the light produced in type-II spontaneous parametric down-conversion in the framework of a multimode model valid in any gain regime. We show that the microscopic polarization entanglement of photon pairs survives in the high gain regime (multiphoton regime), in the form of nonclassical correlation of *all* the Stokes operators describing polarization degrees of freedom.

DOI: 10.1103/PhysRevA.68.053807 PACS number(s): 42.50.Dv, 42.65.Lm

I. INTRODUCTION

The quantum properties of light polarization have been widely studied in the regime of single-photon counts. In comparison, only recently there has been a rise in interest towards the quantum properties of the polarization of macroscopic light beams [1–4], mainly due to their potential applications to the field of quantum information with continuous variables and to the possibility of mapping the quantum state from light to atomic media [5]. A well-known source of polarization-entangled photons is parametric down-conversion in a type-II crystal. Here, a pump field at high frequency is partially converted into two fields at lower frequency, distinguished by their polarizations. Due to spatial walk-off in the crystal, the two emission cones are slightly displaced one with respect to the other, and the far-field intensity distribution has the shape of two rings, whose centers are displaced along the walk-off direction, as, e.g., shown by Fig. 1. The two regions where the far-field rings intersect have a very special role. In the regime where single pairs of atoms are detected, the polarization of a photon detected in one of these regions is completely undetermined. However, once the polarization of one photon has been measured, the polarization of the other photon, which propagates at the symmetric position, is exactly determined. In other words, when considering photodetection from these regions, the two-photon state can be described as the ideal polarization-entangled state [6]. Photons produced by this process have become an essential ingredient in many implementations of quantum information schemes (see, e.g., Refs. [7,8]).

The question that we address in this paper is whether the microscopic photon polarization entanglement leaves any trace in the regime of high parametric down-conversion efficiency, where the number of down-converted photons can be rather large [9], and in which form.

To this end parametric down-conversion is described in the framework of a multimode model, valid for any gain regime, which includes typical effects present in a realistic crystal, as diffraction and spatiotemporal walk-off. Quantum-optical polarization properties of the down-converted light are described within the formalism of Stokes operators. These operators obey angular momentumlike commutation rules, and the associated observables are in general noncompatible. We define a local version of Stokes operators and study the quantum correlation between Stokes operators measured from symmetric portions of the beam cross section in the far-field zone. In the regions where the two down-conversion cones intersect we find that all the Stokes operators are correlated at the quantum level. Although the light is completely unpolarized and Stokes operators are very noisy, a measurement of a Stokes parameter in one of these regions in any polarization basis determines the value of the Stokes parameter in the symmetric region within an uncertainty much below the standard quantum limit.

A continuous variable polarization entanglement, in the form of quantum correlation between Stokes operators of two light beams, has been recently demonstrated [3]. In this work the entanglement is of macroscopic nature, and spatial degrees of freedom do not play any role since the beams are single mode. Continuous variable polarization entanglement which takes into account spatial degrees of freedom of light beams is described in Ref. [10], where we study the properties of the light emitted by a type-II optical parametric oscillator below threshold.

The analysis of this paper is rather focused on providing a bridge between the microscopic and the macroscopic domain, since our model is able to describe the polarization entanglement in parametric down-conversion with a continuous passage from the regime of production of single pairs of photons to the regime of high down-conversion efficiency.

Besides its fundamental interest, we believe that the form of entanglement described in this work can be quite promising for new quantum information schemes, due to the increased number of degrees of freedom in play (photon num-

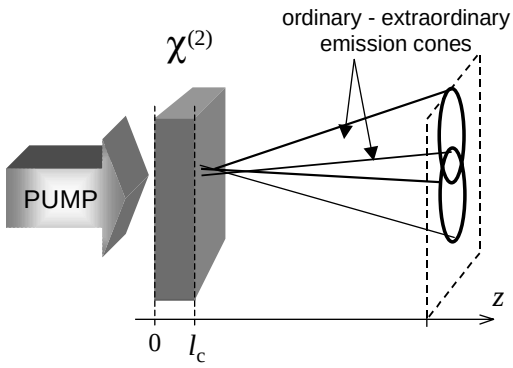

FIG. 1. Parametric down-conversion from a type-II crystal showing the two down-conversion cones at degeneracy.

ber, polarization, frequency, and spatial degrees of freedom), and is well inserted in the recent trend toward entangled state of increasing complexity (see, e.g., Ref. [11], where a four-photon polarization-entangled state is characterized)

The paper is organized as follows. Section II describes the model for spontaneous parametric down-conversion, in terms of propagation equations for field operators. Similar models are known in literature (see, e.g., Ref. [12] and references quoted therein), but besides presenting it in a systematic way, we include all the relevant features of propagation through a nonlinear crystal and provide a precise link with the empirical parameters of real crystals. Section III is devoted to the description of the quantum polarization properties of the down-converted light. Stokes operators' definition and properties are briefly reviewed in Sec. III A. In Sec. III B we generalize this definition to a local measurement in the beam far-field plane and introduce the spatial correlation functions of interest. Analytical and numerical results for the degree of correlation of the various Stokes parameters detected from symmetric portions of the beam cross section are presented in Secs. III C and III D, both in the case when a narrow frequency filter is employed (Sec. III D 1) and when the filter is broadband (Sec. III D 2). Section IV provides an alternative description of the system and of its polarization correlations in the framework of the quantum-state formalism. Section V finally concludes.

II. A MULTIMODE MODEL FOR TYPE-II PARAMETRIC DOWN-CONVERSION

A. Field propagation

The starting point of our analysis is an equation describing the propagation of the three waves (signal, idler, and pump) inside a nonlinear $\chi^{(2)}$ crystal. We consider a crystal slab of length l_c, ideally infinite in the transverse directions, cut for type-II quasicollinear phase matching. In the framework of the slowly varying envelope approximation the electric-field operator associated with the three waves is described by means of three quasimonochromatic wave packets. We take the z axis as the laser pump mean propagation direction (Fig. 1), and indicate with $\vec{x}=(x,y)$ the position coordinates in a generic transverse plane. $\hat{E}_i^{(+)}(z,\vec{x},t)$, $i=o,e,p$ designate the positive frequency part of the field operator (with dimensions of a photon annihilation operator) associated with the ordinary ($i=o$, the "signal") and extraordinary ($i=e$, the "idler") polarization components of the down-converted beam, and ($i=p$ the "pump") the high-frequency laser beam activating the down-conversion process. Next we introduce their Fourier transform in time and in the transverse domain:

$$\hat{A}_i(z,\vec{q},\Omega)=\int \frac{d\vec{x}}{2\pi}\int \frac{dt}{\sqrt{2\pi}} e^{-i\vec{q}\cdot\vec{x}} e^{i(\omega_i+\Omega)t}\hat{E}_i^{(+)}(z,\vec{x},t), \qquad i=o,e,p. \quad (1)$$

Here $\vec{q}$ is the transverse component of the wave vector and Ω represents the frequency offset from the carriers $\omega_o+\omega_e=\omega_p$. In the following, we shall assume degenerate phase matching, so that $\omega_o=\omega_e=\omega_p/2$. It is convenient to subtract from the field operators the fast variation along z arising from linear propagation inside the birefringent crystal. We write

$$\hat{A}_i(z,\vec{q},\Omega)=\exp[ik_{iz}(\vec{q},\Omega)z]\hat{a}_i(z,\vec{q},\Omega), \quad (2)$$

where $k_{iz}(\vec{q},\Omega)=\sqrt{k_i^2(\vec{q},\omega_i+\Omega)-q^2}$ is the projection of the wave vector along the z direction, with $k_i(\vec{q},\omega_i+\Omega)$ being the wave number of the ith wave. In the absence of any nonlinear interaction, we would have

$$\frac{d}{dz}\hat{a}_i(z,\vec{q},\Omega)=0, \quad (3)$$

Eq. (2) with $\hat{a}_i(z,\vec{q},\Omega)=\hat{a}_i(z=0,\vec{q},\Omega)$ being the forward solution of Maxwell wave equation in linear dispersive media. For the pump wave, we assume that the intense laser pulse is undepleted by the down-conversion process, so that $\hat{a}_p(z,\vec{q},\Omega)=\hat{a}_p(z=0,\vec{q},\Omega)$. Moreover, we assume that the pump is an intense coherent beam and the operator can be replaced by its classical mean value $\alpha_p(\vec{q},\Omega)$.

For the signal and idler beams, the variation of $\hat{a}_i$ operators along z is only due to the nonlinear term, proportional to the $\chi^{(2)}$ material second-order susceptibility. This is usually very small, so that $\hat{a}_i$ are slowly varying along z. This allows us to neglect the second-order derivative with respect to z in the wave equation. Hence the resulting propagation equation takes the form (see also Ref. [13] for more details, and Ref. [14] for an alternative derivation)

$$\frac{d}{dz}\hat{a}_i(z,\vec{q},\Omega)=\chi\int d\vec{q}'\int d\Omega'\,\alpha_p(\vec{q}+\vec{q}',\Omega+\Omega')\times\hat{a}_j^{\dagger}(z,\vec{q}',\Omega')e^{-i\Delta_{ij}(\vec{q},\vec{q}';\Omega,\Omega')z/l_c}, \qquad i\neq j=o,e, \quad (4)$$

where χ is a parameter proportional to the second-order susceptibilit of the medium, and

$$\Delta_{ij}(\vec{q},\vec{q}';\Omega,\Omega')=l_c[k_{iz}(\vec{q},\Omega)+k_{jz}(\vec{q}',\Omega')-k_{pz}(\vec{q}+\vec{q}',\Omega+\Omega')] \quad (5)$$

is the phase-mismatch function [15]. Equation (4) describes all the possible microscopic processes through which a pump photon of frequency $\omega_p+\Omega+\Omega'$, propagating in the direction $\vec{q}+\vec{q}'$, is annihilated at position z inside the crystal, and gives rise to a signal and an idler photon, with frequencies $\omega_p/2+\Omega$, $\omega_p/2+\Omega'$, and transverse wave vectors $\vec{q},\vec{q}'$, with an overall conservation of energy and transverse momentum. The effectiveness of each process is weighted by the phase-mismatch function (5), which accounts for conservation of the longitudinal momentum. In the limit of an infinitely long crystal, where longitudinal radiation momentum has to be conserved, only those processes for which $\Delta_{ij}=0$

are allowed. For a finite crystal, however, the phase-matching function has finite bandwidths, say q_0 in the transverse domain and Ω_0 in the frequency domain.

Equation (4) couples all the signal and idler spatial and temporal frequencies within the angular bandwidth of the pump $\delta q \approx 1/w_p$, with w_p being the pump beam waist, and within the pump temporal spectrum $\delta\Omega \approx 1/\tau_p$, where τ_p is the pump pulse duration. In general, no analytical solution is available and one has to resort to numerical methods in order to calculate the quantities of interest, as described in Ref. [13].

A limit where analytical results can be obtained is that of a pump waist and a pump duration large enough, so that $\delta q \ll q_0$, $\delta\Omega \ll \Omega_0$. In this case the pump beam can be approximated by a plane wave

$$\alpha_p(\vec{q}+\vec{q}',\Omega+\Omega') \to \alpha_p \delta(\vec{q}+\vec{q}')\,\delta(\Omega+\Omega'). \tag{6}$$

Equation (4) reduces to

$$l_c \frac{d}{dz} a_o(z,\vec{q},\Omega) = \sigma a_e^{\dagger}(z,-\vec{q},-\Omega) e^{-i\Delta(\vec{q},\Omega)z/l_c},$$

$$l_c \frac{d}{dz} a_e(z,-\vec{q},-\Omega) = \sigma a_o^{\dagger}(z,\vec{q},\Omega) e^{-i\Delta(\vec{q},\Omega)z/l_c}, \tag{7}$$

where $\sigma = l_c \chi \alpha_p$ is a linear gain parameter, and

$$\Delta(\vec{q},\Omega) = l_c[k_{oz}(\vec{q},\Omega) + k_{ez}(-\vec{q},-\Omega) - k_p] \tag{8}$$

is the phase mismatch of a couple of ordinary and extraordinary waves propagating with symmetric transverse wave vectors $\vec{q}$ and $-\vec{q}$, and with frequencies $\omega_p/2+\Omega$, $\omega_p/2-\Omega$.

Solution of the propagation equation (7) is found in terms of the field distributions at the input face of the crystal. Coming back to the field operators defined by Eq. (1), we define the field operators at the input and output faces of the crystal slab as

$$\hat{A}_i^{in}(\vec{q},\Omega) = \hat{a}_i(z=0,\vec{q},\Omega), \tag{9}$$

$$\hat{A}_i^{out}(\vec{q},\Omega) = \hat{a}_i(z=l_c,\vec{q},\Omega)\exp[ik_{iz}(\vec{q},\Omega)l_c]. \tag{10}$$

By solving Eq. (7) the transformation from the input to the output operators is found in the form of a two-mode squeezing transformation:

$$\hat{A}_o^{out}(\vec{q},\Omega) = U_o(\vec{q},\Omega)\hat{A}_o^{in}(\vec{q},\Omega) + V_o(\vec{q},\Omega)\hat{A}_e^{\dagger in}(-\vec{q},-\Omega),$$

$$\hat{A}_e^{out}(\vec{q},\Omega) = U_e(\vec{q},\Omega)\hat{A}_e^{in}(\vec{q},\Omega) + V_e(\vec{q},\Omega)\hat{A}_o^{\dagger in}(-\vec{q},-\Omega), \tag{11}$$

linking only symmetric modes $\vec{q},\Omega$ and $-\vec{q},-\Omega$ in the signal and idler beams (see, e.g., Ref. [12] for a similar transformation in the type-I case). If we require that free space commutation relations

$$[\hat{A}_i^{in}(\vec{q},\Omega),\hat{A}_j^{in}(\vec{q}',\Omega')] = \delta_{i,j}\delta(\vec{q}-\vec{q}')\,\delta(\Omega-\Omega'),$$

$$i,j = o,e \tag{12}$$

are preserved from the input to the output, it can be easily shown that the complex coefficients of transformation (11) need to satisfy the following conditions:

$$|U_i(\vec{q},\Omega)|^2 - |V_i(\vec{q},\Omega)|^2 = 1 \quad (i=o,e), \tag{13}$$

$$U_o(\vec{q},\Omega)V_e(-\vec{q},-\Omega) = V_o(\vec{q},\Omega)U_e(-\vec{q},-\Omega). \tag{14}$$

By taking the modulus of the second relation and making use of the first two ones, the complex equation (14) can be written as two equivalent real equations:

$$|V_o(\vec{q},\Omega)|^2 = |V_e(-\vec{q},-\Omega)|^2, \tag{15}$$

$$\arg[U_o(\vec{q},\Omega)V_e(-\vec{q},-\Omega)] = \arg[V_o(\vec{q},\Omega)U_e(-\vec{q},-\Omega)]$$

$$:= 2\psi(\vec{q},\Omega). \tag{16}$$

With this in mind, the coefficients of transformation (11) can be recasted in the form

$$U_o(\vec{q},\Omega) = U(\vec{q},\Omega)e^{i\varphi(\vec{q},\Omega)}, \quad V_o(\vec{q},\Omega) = V(\vec{q},\Omega)e^{i\varphi(\vec{q},\Omega)},$$

$$U_e(\vec{q},\Omega) = U(-\vec{q},-\Omega)e^{-i\varphi(-\vec{q},-\Omega)},$$

$$V_e(\vec{q},\Omega) = V(-\vec{q},-\Omega)e^{-i\varphi(-\vec{q},-\Omega)}, \tag{17}$$

with

$$U(\vec{q},\Omega) = \cosh r(\vec{q},\Omega)e^{i\psi(\vec{q},\Omega)}e^{i\theta(\vec{q},\Omega)},$$

$$V(\vec{q},\Omega) = \sinh r(\vec{q},\Omega)e^{i\psi(\vec{q},\Omega)}e^{-i\theta(\vec{q},\Omega)}, \tag{18}$$

where $r(\vec{q},\Omega),\varphi(\vec{q},\Omega),\psi(\vec{q},\Omega),\theta(\vec{q},\Omega)$, are independent real functions of $\vec{q},\Omega$.

We outline that the form of transformation (11), together with the unitarity requirements (13) and (14), is enough to derive the general form of the results presented in this paper. In the following, we shall present results for a specific device, namely traveling-wave parametric down-conversion, and we shall take as an example the case of a BBO (*beta*-barium-borate) crystal. However, a similar investigation can be carried out for any device characterized by an input/ouput transformation of form (11). The case of type-II parametric down-conversion inside an optical resonator is for example investigated in Ref. [10].

More insight into the problem is gained by looking at the explicit solution of the propagation equation (7). We obtain

$$U(\vec{q},\Omega) = e^{i(k_p l_c/2)}\left\{\cosh[\Gamma(\vec{q},\Omega)] + i\frac{\Delta(\vec{q},\Omega)}{2\Gamma(\vec{q},\Omega)}\sinh[\Gamma(\vec{q},\Omega)]\right\}, \tag{19}$$

$$V(\vec{q},\Omega)=e^{i(k_p l_c/2)}\frac{\sigma}{\Gamma(\vec{q},\Omega)}\sinh[\Gamma(\vec{q},\Omega)], \tag{20}$$

$$\varphi(\vec{q},\Omega)=\frac{l_c}{2}[k_{oz}(\vec{q},\Omega)-k_{ez}(-\vec{q},-\Omega)], \tag{21}$$

with

$$\Gamma(\vec{q},\Omega)=\sqrt{\sigma^2-\frac{\Delta^2(\vec{q},\Omega)}{4}}, \tag{22}$$

and $\Delta(\vec{q},\Omega)$ is the phase-mismatch function defined by Eq. (8).

B. Phase-matching curves

The gain functions (19) and (20) reach their maximum value for phase-matched modes, that is, the modes for which $\Delta(\vec{q},\Omega)=0$. By assuming the validity of the paraxial and slowly varying envelope approximations, the longitudinal wave-vector components $k_{iz}(\vec{q},\Omega)$ can be expanded in power series of $\vec{q},\Omega$. By keeping only the leading terms we obtain

$$k_{iz}(\vec{q},\Omega)\approx k_i+\frac{1}{v_g^i}\Omega+\frac{1}{2}\frac{d^2k_i}{d\Omega^2}\Omega^2+\frac{dk_i}{dq_y}q_y-\frac{q^2}{2k_i},\quad i=o,e. \tag{23}$$

The first term at on the right-hand side (rhs) is $k_i=n_i(\omega_i,\vec{q}=0)\omega_i/c$, with n_i being the index of refraction at the carrier frequency of an ordinary (extraordinary) wave propagating along z direction. The second term $(1/v_g^i)\Omega=(dk_i/d\Omega)\Omega$ accounts for the fact that the three wave packets move with different group velocities v_g^i. The third term describes the effects of temporal dispersion. In writing the fourth term, we assumed that the crystal is uniaxial and the crystal optical axis lies in the z-y plane. This term is present only for the extraordinary waves, and $dk_i/dq_y=-\rho_i$ where ρ_i is the walk-off angle of the wave. Finally, the last term describes the effects of diffraction for a paraxial wave.

With this in mind, the phase-matching function can be written in the form

$$\Delta(\vec{q},\Omega)=\Delta_0+\rho_e l_c q_y-\frac{q^2}{q_0^2}+\Omega\tau_{coh}+\frac{1}{2}\epsilon(\Omega\tau_{coh})^2, \tag{24}$$

where

$$\Delta_0=(k_o+k_e-k_p)l_c \tag{25}$$

is the collinear phase-mismatch (i.e., the phase mismatch of the three waves at the carrier frequencies when propagating along the longitudinal direction);

$$q_0=\sqrt{\frac{1}{l_c}\frac{k_e+k_o}{2k_ek_o}}=\sqrt{\frac{2\pi}{\lambda l_c}\frac{n_e+n_o}{2n_en_o}} \tag{26}$$

with $\lambda=4\pi c/\omega_p$ being the wavelength in vacuum at the carrier frequency $\omega_p/2$, and n_e,n_o the ordinary and extraordinary refraction indices inside the crystal at the carrier frequency. This parameter defines the typical bandwidth of phase matching in the transverse q-space domain. Its inverse $l_{coh}=1/q_0$ will be referred to as the *coherence length*;

$$\tau_{coh}=\frac{l_c}{v_g^o}-\frac{l_c}{v_g^e}, \tag{27}$$

with v_g^i being the group velocities of the two waves, is the difference between the time taken by the signal and idler wave packets to cross the crystal. This defines the typical scale of variation of gain functions in the temporal domain for type-II phase matching, and it will be referred to as the amplifier *coherence time*; finally

$$\epsilon=\left(\frac{d^2k_o}{d\Omega^2}+\frac{d^2k_e}{d\Omega^2}\right)\frac{l_c}{\tau_{coh}^2} \tag{28}$$

is a dimensionless parameter that depends on the temporal dispersion properties of the signal and idler pulses (typically $\epsilon\ll 1$).

The equation $\Delta(\vec{q},\Omega)=0$ defines in the (q_x,q_y) plane a circumference, centered at the position

$$q_x=0,\quad q_y=q_C=\tfrac{1}{2}q_0^2\rho_e l_c \tag{29}$$

and with radius given by

$$q_R=q_0\sqrt{\Delta_0+\frac{q_C^2}{q_0^2}+\Omega\tau_{coh}+\frac{1}{2}\epsilon(\Omega\tau_{coh})^2}. \tag{30}$$

This corresponds to the phase-matched modes for the signal (ordinary) wave. Phase-matched modes for the idler wave, emitted at the frequency $-\Omega$, lie on the symmetric circumference.

Figure 2 plots an example of these phase-matching circles, in the form of polar plot, with θ being the polar angle from the pump direction (z axis) outside the crystal and ϕ the azimuthal angle around z. Parameters are those of a 2-mm-long BBO crystal, cut for degenerate phase matching at 49.6°, for a pump wavelength of 351 nm. They have been calculated with the help of empirical Sellmeier formulas for refraction indices in Ref. [16]. In the degenerate case, for a signal and idler wavelength of 702 nm, the relevant parameters are as follows: idler (extraordinary wave) walk-off angle $\rho_e=4.06°$; $\Delta_0=16.137$; $q_0=0.0853\ \mu\mathrm{m}^{-1}$, with a transverse coherence length $l_{coh}\approx 11.7\ \mu$m; $\tau_{coh}\approx 0.44$ ps; $\epsilon=1.7\times10^{-3}$. With the exception of Δ_0, which varies rather rapidly even for small variations of refraction indices, all the other parameters vary rather slowly with the pump angle and signal-idler wavelengths, so that the above numbers give the typical order of magnitude of the parameters of a BBO crystal of this length.

For comparison, superimposed to the curves calculated by means of Eq. (24), the figure shows the ''exact'' phase-matching curves, calculated with the method described in

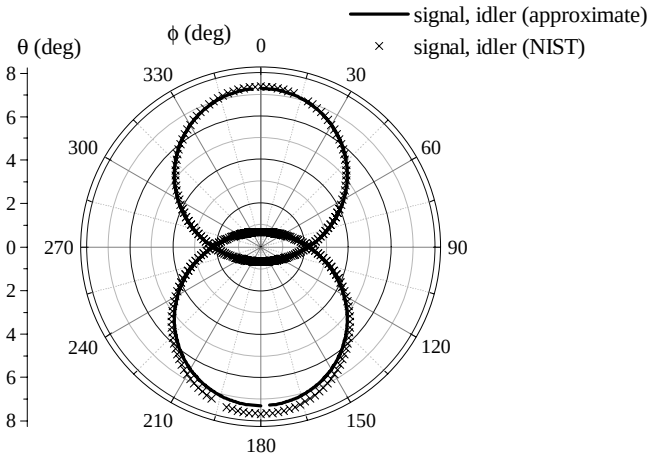

FIG. 2. Polar plot of phase-matching curves in a BBO crystal. Comparison of the approximated formula (24) with the "exact" phase-matching formula, calculated with the method in Ref. [17] (NIST). θ is the polar angle from the pump direction of propagation, ϕ is the azimuthal angle. $\lambda_{signal}=\lambda_{idler}=702$ nm. ($\lambda_{pump}=351$ nm), and the pump propagates at an angle of 49.6° from the crystal optical axis. Signal (ordinary) curves are in the upper half of the plot, idler (extraordinary) in the lower half.

Ref. [17], by means of a public domain numerical routine available in Ref. [18]. The plots show a rather good agreement, in any case within the error implicit in the use of empirical Sellmeier formulas.

III. POLARIZATION CORRELATION: QUANTUM-FIELD FORMALISM

A. Stokes operators: definition and properties

Quantum-optical polarization properties of light are conveniently described within the formalism of Stokes operators, which represent the quantum counterparts of the Stokes vectors of classical optics. The polarization state of a classical beam can be described by means of a Stokes vector, and of its associated Poincaré sphere. Stokes vectors pointing on the equator of the sphere represent linearly polarized light; if the vector points in the positive (negative) direction of S_1 the light is horizontally (vertically) polarized, while the S_2 direction identifies light polarized at 45° ($-45°$). The S_3 direction corresponds to circularly (right and left) polarized light. A fourth parameter S_0 is the total beam intensity, and gives the radius of the Poincaré sphere. For a polarized beam $S_1^2+S_2^2+S_3^2=S_0^2$, so that the polarization state is represented by a point on the sphere surface.

In the quantum-mechanical description of light polarization, Stokes parameters are replaced by a set of four Stokes operators. For a single mode of an electromagnetic field, they are defined in terms of the photon annihilation operators for a vertical and a horizontal linear polarization mode $\hat{a}_H,\hat{a}_V$, as

$$\hat{S}_0=\hat{a}_H^\dagger\hat{a}_H+\hat{a}_V^\dagger\hat{a}_V, \tag{31}$$

$$\hat{S}_1=\hat{a}_H^\dagger\hat{a}_H-\hat{a}_V^\dagger\hat{a}_V, \tag{32}$$

$$\hat{S}_2=\hat{a}_H^\dagger\hat{a}_V+\hat{a}_V^\dagger\hat{a}_H=\hat{a}_{45}^\dagger\hat{a}_{45}-\hat{a}_{-45}^\dagger\hat{a}_{-45}, \tag{33}$$

$$\hat{S}_3=-i(\hat{a}_H^\dagger\hat{a}_V-\hat{a}_V^\dagger\hat{a}_H)=\hat{a}_R^\dagger\hat{a}_R-\hat{a}_L^\dagger\hat{a}_L, \tag{34}$$

where $\hat{a}_{45},\hat{a}_{-45}$ denote annihilation operators on the oblique polarization basis, and a_R,a_L are annihilation operators on the circular right and circular left polarization basis. The first two operators represent, respectively, the sum and differences of photon numbers in the vertical/horizontal polarization basis. Operators $\hat{S}_2$ and $\hat{S}_3$ are the differences of photon numbers in the oblique and circular polarization basis, respectively. All these observables can be measured by means of a polarizing beam splitter and quarter- and half-wave plates, as, e.g., described in Ref. [19]. However, while operator $\hat{S}_0$ commutes with all the others, the remaining three do not:

$$[\hat{S}_1,\hat{S}_2]=2i\hat{S}_3,\quad [\hat{S}_2,\hat{S}_3]=2i\hat{S}_1,\quad [\hat{S}_3,\hat{S}_1]=2i\hat{S}_2. \tag{35}$$

The set of Stokes operators has angular-momentum-like commutation relation, and the associated observables are in general noncompatible. The quantum state of a light beam cannot be anymore visualized as a point on the Poincaré sphere, since quantum noise introduces a minimum uncertainty in the values of the Stokes parameter. Polarization squeezed states, whose uncertainty can be represented by an ellipsoid (see, e.g., Ref. [2]), have been recently realized [1].

B. Stokes operator correlation in the far field of parametric down-conversion

The main idea of this paper is to study the quantum correlation between Stokes operators measured from symmetric portions of the far-field beam cross section. To this end, we consider a measurement of the Stokes operators over a small region $D(\vec{x})$ centered around a position $\vec{x}$ in the far-field plane of the down-converted field, and over a detection time T (typically T is much larger than the crystal coherence time):

$$\hat{S}_i(\vec{x})=\int_T dt'\int_{D(\vec{x})}d\vec{x}'\,\hat{\sigma}_i(\vec{x}',t'), \tag{36}$$

where

$$\hat{\sigma}_0(\vec{x},t)=\hat{A}_o^\dagger(\vec{x},t)\hat{A}_o(\vec{x},t)+\hat{A}_e^\dagger(\vec{x},t)\hat{A}_e(\vec{x},t), \tag{37}$$

$$\hat{\sigma}_1(\vec{x},t)=\hat{A}_o^\dagger(\vec{x},t)\hat{A}_o(\vec{x},t)-\hat{A}_e^\dagger(\vec{x},t)\hat{A}_e(\vec{x},t), \tag{38}$$

$$\hat{\sigma}_2(\vec{x},t)=\hat{A}_o^\dagger(\vec{x},t)\hat{A}_e(\vec{x},t)+\hat{A}_e^\dagger(\vec{x},t)\hat{A}_o(\vec{x},t), \tag{39}$$

$$\hat{\sigma}_3(\vec{x},t)=-i[\hat{A}_o^\dagger(\vec{x},t)\hat{A}_e(\vec{x},t)-\hat{A}_o^\dagger(\vec{x},t)\hat{A}_e(\vec{x},t)]. \tag{40}$$

$\hat{A}_{o/e}$ denotes the field operator for the ordinary/extraordinary polarized beam in the far-field plane, which can be observed in the focal plane of a lens, placed as shown in Fig. 3.

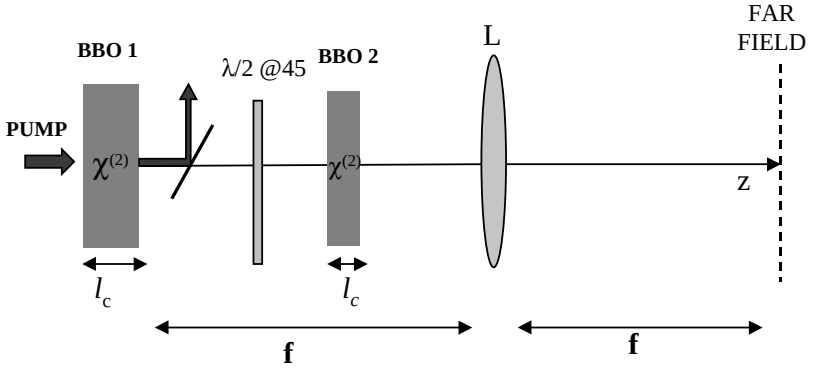

FIG. 3. Schematic setup for a measurement in the far-field plane with a compensation crystal. BBO1, down-conversion crystal of length l_c; λ/2@45 half-wave plate rotates polarization by 90°; BBO2, compensation crystal of length l_c', L lens of focal length f.

By using the free field commutation relations (12), it can be easily shown that

$$[\hat{S}_1(\vec{x}),\hat{S}_2(\vec{x})]=2i\hat{S}_3(\vec{x}),\quad [\hat{S}_2(\vec{x}),\hat{S}_3(\vec{x})]=2i\hat{S}_1(\vec{x}),$$
$$[\hat{S}_3(\vec{x}),\hat{S}_1(\vec{x})]=2i\hat{S}_2(\vec{x}), \tag{41}$$

while operators measured from different (and not connectedy detection pixels commute.

In the following, we shall consider Stokes operator correlation functions of the form

$$\langle \delta\hat{S}_i(\vec{x})\,\delta\hat{S}_j(\vec{x}')\rangle=\langle \hat{S}_i(\vec{x})\hat{S}_j(\vec{x}')\rangle-\langle \hat{S}_i(\vec{x})\rangle\langle \hat{S}_j(\vec{x}')\rangle$$
$$(i,j=0,\ldots,3). \tag{42}$$

A useful tool for calculation is the correlation functions of the Stokes operator densities (37)–(40):

$$G_{ij}(\vec{x},\vec{x}';\tau)=\langle \hat{\sigma}_i(\vec{x},t+\tau)\hat{\sigma}_j(\vec{x}',t)\rangle-\langle \hat{\sigma}_i(\vec{x},t+\tau)\rangle$$
$$\times\langle \hat{\sigma}_j(\vec{x}',t)\rangle. \tag{43}$$

In the continous-wave pump regime the system is stationary in time and the correlation functions (43) depend only on the time delay τ. Spectral densities of these functions can be introduced as

$$\tilde{G}_{ij}(\vec{x},\vec{x}';\Omega)=\int d\tau e^{i\Omega\tau}G_{ij}(\vec{x},\vec{x}';\tau). \tag{44}$$

Their relation with the correlation functions of the measured Stokes operator (42) is given by

$$\langle \delta\hat{S}_i(\vec{x})\,\delta\hat{S}_j(\vec{x}')\rangle=\int_{D(\vec{x})}d\vec{x}_1\int_{D(\vec{x}')}d\vec{x}_1'\int d\Omega\frac{T^2}{2\pi}\sin c^2\left(\Omega\frac{T}{2}\right)$$
$$\times\tilde{G}_{ij}(\vec{x}_1,\vec{x}_1';\Omega). \tag{45}$$

We notice that

$$\lim_{T\to\infty}\frac{T}{2\pi}\sin c^2\left(\Omega\frac{T}{2}\right)=\delta(\Omega), \tag{46}$$

and that this function acts under the integral as a frequency filter with bandwidth $\Delta\Omega=2\pi/T$. We shall assume in the following that the detection time is much larger than the crystal coherence time. Under this assumption

$$\langle \delta\hat{S}_i(\vec{x})\,\delta\hat{S}_j(\vec{x}')\rangle\xrightarrow{T\gg\tau_{coh}}T\int_{D(\vec{x})}d\vec{x}_1\int_{D(\vec{x}')}d\vec{x}_1'$$
$$\times\tilde{G}_{ij}(\vec{x}_1,\vec{x}_1';\Omega=0). \tag{47}$$

When a lens of focal length f is placed at a focal distance both from the crystal output plane and the observation plane (see Fig. 3), the field operators in the far-field plane are connected to those at the crystal output by the usual mapping [20]

$$\hat{A}_i(\vec{x},\Omega)=\frac{2\pi}{i\lambda_i f}\hat{A}_i^{out}\left(\vec{q}=\frac{2\pi\vec{x}}{\lambda_i f},\Omega\right), \tag{48}$$

where f is the focal length of the lens used to image the far-field plane and λ_i is the wavelength (in vacuum) at the frequency $\omega_p/2+\Omega$.

Since the light statistics is Gaussian (the output operators are obtained by a linear transformation acting on input vacuum field operators) all expectation values and correlation functions of interest can be calculated by making use of the second-order moments of field operators. These can be easily calculated in the far-field plane by assuming that the down-converted field operators at the input crystal face are in the vacuum state and by using the input/output relations (11), together with Eq. (48), thus obtaining

$$\langle \hat{A}_i^\dagger(\vec{x},\Omega)\hat{A}_j(\vec{x}',\Omega')\rangle=\delta_{i,j}\delta(\vec{x}-\vec{x}')\,\delta(\Omega-\Omega')|\mathcal{V}_i(\vec{x},\Omega)|^2, \tag{49}$$

$$\langle \hat{A}_i(\vec{x},\Omega)\hat{A}_j(\vec{x}',\Omega')\rangle=-\frac{\lambda_j}{\lambda_i}(1-\delta_{i,j})\,\delta\left(\vec{x}\frac{\lambda_j}{\lambda_i}+\vec{x}'\right)$$
$$\times\delta(\Omega+\Omega')\mathcal{U}_i(\vec{x},\Omega)$$
$$\times\mathcal{V}_j\left(-\vec{x}\frac{\lambda_j}{\lambda_i},-\Omega\right)\quad(i,j=o,e). \tag{50}$$

In this formula

$$\mathcal{U}_i(\vec{x},\Omega)=U_i\left(\vec{q}=\vec{x}\frac{2\pi}{\lambda_i f},\Omega\right),\quad \mathcal{V}_i(\vec{x},\Omega)=V_i\left(\vec{q}=\vec{x}\frac{2\pi}{\lambda_i f},\Omega\right), \tag{51}$$

where U_i, V_i are are the gain functions defined by Eqs. (17)–(22). Notice the presence of the nonzero "anomalous" propagator described by Eq. (50), a term which is characteristic of processes where particles are created in pairs. In order to simplify the notation, in the following we shall consider the case $\Omega \ll \omega_p/2$, and take $\lambda_o=\lambda_e=\lambda=2\lambda_p$. In a real experimental implementation, however, the validity of such an approximation should be carefully checked when not using narrow frequency filters; twin photons produced at different wavelengths λ_e, λ_o, and traveling with symmetric $\vec{q}$, $-\vec{q}$ transverse wave vectors are actually propagating at different angles from the pump and will be intercepted in the far field at two slightly different radial positions.

The fact that the field spatial correlations are perfectly localized in the far field (the Dirac-δ form of the correlation peak) is a consequence of the translational symmetry of the model in the transverse plane (plane-wave pump and a crystal slab infinite in the transverse direction). A trivial formal fault is that the far-field mean intensity of the down-converted beams diverges as a consequence of the infinite energy of a plane-wave pump. This artificial divergence can be formally eliminated with the trick used in Refs. [21,22], where a finite-size pupil was inserted at the output face of the crystal. The spatial Dirac-δ functions in Eqs. (49) and (50) are substituted by a finite version, and a typical resolution area, proportional to the diffraction spot of the pupil in the far-field plane, is introduced in the scheme. For a pupil of transverse area S_P, this is given by $D_R=(\lambda f)^2/S_P$. The typical scale of variation of the gain functions (51) in the far-field plane is

$$X_0=q_0\frac{\lambda f}{2\pi}. \tag{52}$$

When X_0 is much larger than the resolution area (or, equivalently, when the pupil size is much larger than the amplifier coherence length), the mean photon number distribution in the far-field plane is given by

$$\langle \hat{N}_i(\vec{x})\rangle=\int_{D(\vec{x})}d\vec{x}'\int_T dt\langle \hat{A}_i^\dagger(\vec{x}',t)\hat{A}_i(\vec{x}',t)\rangle \approx\frac{T}{D_R}\int_{D(\vec{x})}d\vec{x}'\int\frac{d\Omega}{2\pi}|\mathcal{V}_i(\vec{x}',\Omega)|^2. \tag{53}$$

When the finite size of the pump is taken into account in a numerical model [13], it is easily seen that the resolution area is rather given in terms of the spot size of the pump as it is imaged in the far-field plane. For a Gaussian pump of waist w_p, $D_R\approx(\lambda f)^2/(\pi w_p^2)$.

In this limit of small resolution area, the mean value of Stokes operators is given by

$$\langle \hat{S}_0(\vec{x})\rangle=\frac{T}{D_R}\int_{D(\vec{x})}d\vec{x}'\int\frac{d\Omega}{2\pi}[|\mathcal{V}_o(\vec{x}',\Omega)|^2+|\mathcal{V}_e(\vec{x}',\Omega)|^2], \tag{54}$$

$$\langle \hat{S}_1(\vec{x})\rangle=\frac{T}{D_R}\int_{D(\vec{x})}d\vec{x}'\int\frac{d\Omega}{2\pi}[|\mathcal{V}_o(\vec{x}',\Omega)|^2-|\mathcal{V}_e(\vec{x}',\Omega)|^2], \tag{55}$$

$$\langle \hat{S}_2(\vec{x})\rangle=\langle \hat{S}_3(\vec{x})\rangle=0. \tag{56}$$

C. Correlation in Stokes operators S_1, S_0

The first and second Stokes operators represent the sum and the difference, respectively, between the number of ordinary and extraordinary photons (say horizontally and vertically polarized photons) measured from a detection pixel in the far-field plane:

$$\hat{S}_0(\vec{x})=\hat{N}_o(\vec{x})+\hat{N}_e(\vec{x}), \tag{57}$$

$$\hat{S}_1(\vec{x})=\hat{N}_o(\vec{x})-\hat{N}_e(\vec{x}). \tag{58}$$

The plane-wave pump model predicts that the number of ordinary and extraordinary photons collected from any two symmetric portions of the far-field plane are perfectly correlated observables [13,21]. This result is a direct consequence of pairwise emission of photons with horizontal (ordinary) and vertical (extraordinary) polarizations, propagating in symmetric directions, as required by transverse light momentum conservation. Hence, this model predicts an ideally perfect correlation, both between $\hat{S}_0(\vec{x}), \hat{S}_0(-\vec{x})$, and between $\hat{S}_1(\vec{x}), -\hat{S}_1(-\vec{x})$ for any choice of the position $\vec{x}$ in the far field [notice that $\hat{S}_0(\vec{x})$ commutes with $\hat{S}_1(\vec{x}')$].

In a more sophisticated numerical model [13], it is readily seen that the finite width of the pump profile introduces an uncertainty in the directions of propagation of the down-converted photons. As described by the propagation equation (4), when an *o* photon is emitted in direction $\vec{q}$, its twin *e* photon is emitted in the direction $-\vec{q}$ within an uncertainty $\delta q\propto 2/w_p$, which is the bandwidth of the pump spatial Fourier transform. A photon number correlation well beyond the shot-noise level is recovered when photons are collected from regions larger than a resolution area

$$D_R\approx\pi\left(\delta q\frac{\lambda f}{2\pi}\right)^2=(\lambda f)^2/(\pi w_p^2).$$

In the limit of a small resolution area, long but straightforward calculations [23] show that

$$\tilde{G}_{00}(\vec{x},\vec{x}';\Omega)=\frac{1}{D_R}[\delta(\vec{x}-\vec{x}')F_1(\vec{x},\Omega)+\delta(\vec{x}+\vec{x}')F_2(\vec{x},\Omega)], \tag{59}$$

$$\tilde{G}_{11}(\vec{x},\vec{x}';\Omega)=\frac{1}{D_R}[\delta(\vec{x}-\vec{x}')F_1(\vec{x},\Omega)-\delta(\vec{x}+\vec{x}')F_2(\vec{x},\Omega)] \tag{60}$$

with

$$F_1(\vec{x},\Omega)=\int \frac{d\omega}{2\pi}\{|\mathcal{V}_o(\vec{x},\omega)\mathcal{U}_o(\vec{x},\omega+\Omega)|^2 + |\mathcal{V}_e(\vec{x},\omega)\mathcal{U}_e(\vec{x},\omega+\Omega)|^2\}, \tag{61}$$

$$F_2(\vec{x},\Omega)=\int \frac{d\omega}{2\pi}\{\mathcal{U}_o(\vec{x},\omega)\mathcal{U}_o^*(\vec{x},\omega-\Omega)\mathcal{V}_e(-\vec{x},-\omega) \times\mathcal{V}_e^*(-\vec{x},-\omega+\Omega)+\mathcal{U}_e(\vec{x},\omega)\mathcal{U}_e^*(\vec{x},\omega-\Omega) \times\mathcal{V}_o(-\vec{x},-\omega)\mathcal{V}_0^*(-\vec{x},-\omega+\Omega)\}. \tag{62}$$

The correlation functions have two peaks; the first one, located at $\vec{x}'=\vec{x}$, accounts for the noise in the measurement of Stokes parameter from a single pixel. The second one is located at $\vec{x}'=-\vec{x}$ and accounts for correlation (anticorrelation) between measurements performed over symmetric pixels. By taking into account the unitarity relations (13) and (15), it can be immediately noticed that when $\Omega=0$ (corresponding to long detection times) $F_1(\vec{x},0)=F_2(\vec{x},0)$, and the two correlation function peaks have the same size. This represents the maximum amount of correlation allowed by Schwarz inequality, which requires that

$$|\langle\delta\hat{S}_i(\vec{x})\,\delta\hat{S}_i(-\vec{x})\rangle|\leqslant[\langle\delta\hat{S}_i(\vec{x})\,\delta\hat{S}_i(\vec{x})\rangle\langle\delta\hat{S}_i(-\vec{x}) \times\delta\hat{S}_i(-\vec{x})\rangle]^{1/2}. \tag{63}$$

In our case, assuming two s)mmetric detection pixels $D(\vec{x})$ and $D(-\vec{x})$, we have, e.g.,

$$\langle\delta\hat{S}_1(\vec{x})\,\delta\hat{S}_1(\vec{x})\rangle=\langle\delta\hat{S}_1(-\vec{x})\,\delta\hat{S}_1(-\vec{x})\rangle =\frac{T}{D_R}\int_{D(\vec{x})}d\vec{x}'F_1(\vec{x}',0), \tag{64}$$

$$\langle\delta\hat{S}_1(\vec{x})\,\delta\hat{S}_1(-\vec{x})\rangle=-\frac{T}{D_R}\int_{D(\vec{x})}d\vec{x}'F_2(\vec{x}',0) =-\langle\delta\hat{S}_1(\vec{x})\,\delta\hat{S}_1(\vec{x})\rangle. \tag{65}$$

Finally, the existence of such a perfect correlation implies that both $\hat{S}_1(\vec{x})+\hat{S}_1(-\vec{x})$ and $\hat{S}_0(\vec{x})-\hat{S}_0(-\vec{x})$ are noiseless observables. For example,

$$\langle[\delta\hat{S}_1(\vec{x})+\delta\hat{S}_1(-x)]^2\rangle =2[\langle\delta\hat{S}_1(\vec{x})\,\delta\hat{S}_1(\vec{x})\rangle+\langle\delta\hat{S}_1(\vec{x})\,\delta\hat{S}_1(-\vec{x})\rangle]=0. \tag{66}$$

We remark that the ''twin beam'' character of the down-converted light is recovered only for measurement time long compared with the coherence time and for detection areas broader than the resolution area D_R. This is natural because coherence time and resolution area represent the typical uncertainty in the arrival time and arrival position of the second photon after its twin one has been detected at some far-field position. For what concerns time, typical detection times are much longer than the coherence time, since in a few millimeter type-II crystal $\tau_{coh}\approx 1$ ps. In space, we can assume that for a given down-conversion frequency the typical width X_0 of the down-conversion rings in the far-field is proportional to the emission bandwidth in q space, $X_0\approx q_0\lambda f$. The plane-wave pump results described above hold in the limit where the resolution area is much smaller than X_0^2. We have that $X_0^2/D_R\approx q_0^2w_p^2=(w_p/l_{coh})^2$, and since $l_{coh}\approx 10\ \mu$m, this limit can be easily achieved with a realistic pump size (see Ref. [13] for more details).

D. Correlation in Stokes operators S_2, S_3

Quite different is the situation for the other two Stokes operators S_2, S_3, which involve measurements of the photon number in a polarization basis different from the ordinary and extraordinary ones of the crystal, namely in the oblique and circular polarization basis.

Calculations along the same lines of those performed for the first two Stokes operators show that also in this case the correlation functions display two peaks, one representing the noise associated with the measurement over a single pixel, the other the correlation between symmetric pixels:

$$\tilde{G}_{22}(\vec{x},\vec{x}';\Omega)=\tilde{G}_{33}(\vec{x},\vec{x}';\Omega) \tag{67}$$

$$=\frac{1}{D_R}[\delta(\vec{x}-\vec{x}')H_1(\vec{x},\Omega)+\delta(\vec{x}+\vec{x}')H_2(\vec{x},\Omega)] \tag{68}$$

with

$$H_1(\vec{x},\Omega)=\int \frac{d\omega}{2\pi}\{|\mathcal{V}_o(\vec{x},\omega)\mathcal{U}_e(\vec{x},\omega+\Omega)|^2 + |\mathcal{V}_e(\vec{x},\omega)\mathcal{U}_o(\vec{x},\omega+\Omega)|^2\}, \tag{69}$$

$$H_2(\vec{x},\Omega)=\int \frac{d\omega}{2\pi}\{\mathcal{U}_o^*(\vec{x},\omega)\mathcal{U}_e(\vec{x},\omega+\Omega)\mathcal{V}_e^*(-\vec{x},-\omega) \times\mathcal{V}_o(-\vec{x},-\omega-\Omega)+\mathcal{U}_e^*(\vec{x},\omega)\mathcal{U}_o(\vec{x},\omega+\Omega) \times\mathcal{V}_o^*(-\vec{x},-\omega)\mathcal{V}_e(-\vec{x},-\omega-\Omega)\}. \tag{70}$$

However, unlike the previous case, the two peaks in general do not have the same size, even for a long measurement time. Letting $\Omega=0$ in Eqs. (69) and (70) and using definition (17), which is a consequence of unitarity, we have

$$H_1(\vec{x},0)=\int \frac{d\omega}{2\pi}\{|\mathcal{V}(\vec{x},\omega)\mathcal{U}(-\vec{x},-\omega)|^2 + |\mathcal{V}(-\vec{x},-\omega)\mathcal{U}(\vec{x},\omega)|^2\}, \tag{71}$$

$$H_2(\vec{x},0)=\int \frac{d\omega}{2\pi}2\ \mathrm{Re}\{\mathcal{U}^*(\vec{x},\omega)\mathcal{U}(-\vec{x},-\omega)\mathcal{V}^*(\vec{x},\omega) \times\mathcal{V}(-\vec{x},-\omega)\}, \tag{72}$$

$$H_1(\vec{x},0)-H_2(\vec{x},0)=\int \frac{d\omega}{2\pi}|\mathcal{V}^*(\vec{x},\omega)\mathcal{U}(-\vec{x},-\omega) - \mathcal{V}^*(-\vec{x},-\omega)\mathcal{U}(\vec{x},\omega)|^2, \quad (73)$$

where $\mathcal{U},\mathcal{V}$ appearing in these equations are the functions defined by Eqs. (19) and (20), calculated at $\vec{q}=\vec{x}2\pi/(\lambda f)$. Moreover,

$$\langle[\hat{S}_2(\vec{x})-\hat{S}_2(-\vec{x})]^2\rangle=\langle[\hat{S}_3(\vec{x})-\hat{S}_3(-\vec{x})]^2\rangle \quad (74)$$

$$=\frac{2T}{D_R}\int_{D(\vec{x})} d\vec{x}'[H_1(\vec{x}',0)-H_2(\vec{x}',0)]. \quad (75)$$

The noise in the difference between Stokes operators measured from symmetric pixels in general does not vanish, due to the lack of symmetry $\vec{x},\Omega\rightarrow-\vec{x},-\Omega$ in the gain functions. In turn, this reflects the effect of spatial walk-off between the ordinary/extraordinary beams [described by the term proportional to q_y in the phase-mismatch function (24)] and the group-velocity mismatch between the two waves [described by the term proportional to Ω in Eq. (24)].

In the following two sections we will compare the noise in the difference between Stokes operators from two symmetric detection pixels (74) and (75), with the shot-noise level, that is, the level of noise that would be shown by a coherent beam of the same intensity. This is defined by the equation

$$\langle[\hat{S}_{2,3}(\vec{x})-\hat{S}_{2,3}(-\vec{x})]^2\rangle = \langle[\hat{S}_0(\vec{x})+S_0(-\vec{x})]\rangle+\langle:[\hat{S}_{2,3}(\vec{x})-\hat{S}_{2,3}(-\vec{x})]^2:\rangle, \quad (76)$$

where the first term on the rhs is the shot noise, $\langle::\rangle$ is the normally ordered expectation value that vanishes for a coherent beam, and relation (76) is easily obtained by using the field commutation relations (12). It is not difficult to show that the shot noise represents the level of noise that would affect the difference between the Stokes operators of two light modes obtained by dividing a beam by means of a symmetric beam splitter. In general, the shot noise would affect the noise in the difference between Stokes operators of two modes whose correlations are created by splitting a light beam with such a classical device, and defines the standard quantum limit.

In the following we will show that for proper modes of the down-converted light, a level of correlation well beyond the standard quantum limit can be reached for *all* the Stokes operators at the same time. We will refer to this situation as ''polarization entanglement'' because it represents the natural generalization of the concept of polarization entanglement, commonly used in the coincidence count regime, to the regime of multiple pair production. However, it is important to remark that for spontaneous parametric down-conversion there is no way, to our knowledge, to derive a sufficient criterion for inseparability based on the degree of correlation of the Stokes operators, as that derived in Ref. [24] and generalized in Ref. [3]. This depends on the fact that the average values of commutators (and anticommutators) of Stokes operators are in this system intrinsically state dependent, at difference to what happens in the experiment performed in Ref. [3], where bright entangled beams were used.

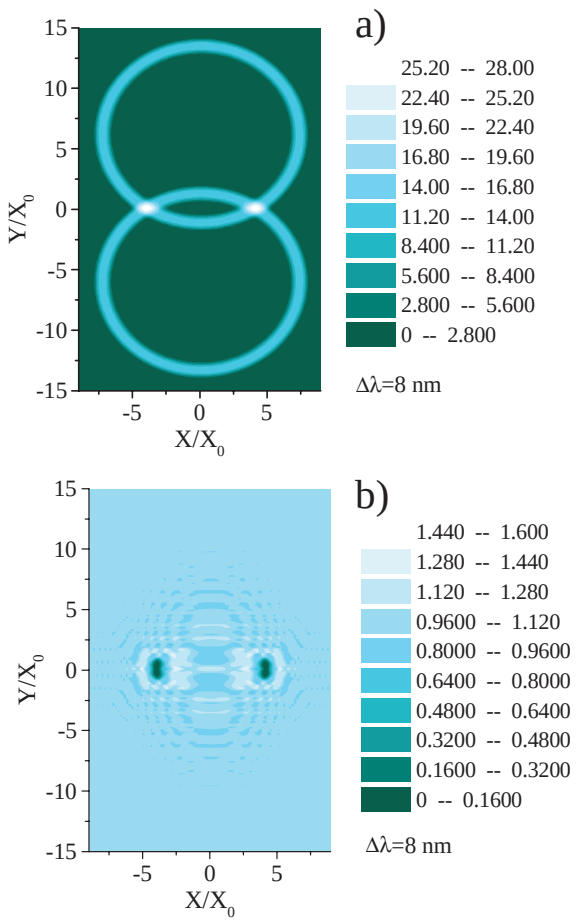

FIG. 4. (a) Far-field photon number distribution of the down-converted field. (b) Distribution of the noise in the difference between $\hat{S}_2$ measured from symmetric portions of the beam cross section, scaled to the shot-noise level. The distribution for $\hat{S}_3$ is identical. A step-function frequency filter $\Delta\lambda=8$ nm wide, centered around the degenerate frequency is used in both plots. $\sigma=2$.

1. Narrow-band frequency filtering results

Part (b) of Fig. 4 shows a typical result for the noise in the difference between Stokes operators measured from small (but larger than D_R) symmetric portions of the far field. Precisely, the figure shows $\langle[\hat{S}_2(\vec{x})-S_2(-\vec{x})]^2\rangle=\langle[\hat{S}_3(\vec{x})-S_3(-\vec{x})]^2\rangle$, scaled to the shot-noise level $\langle[\hat{S}_0(\vec{x})+S_0(-\vec{x})]\rangle$, as a function of the transverse coordinate $\vec{x}=(x,y)$ scaled to X_0. Parameters in this plot are those of a 2-mm-long BBO crystal, cut at 49.6° for degenerate type-II phase matching at 702 nm. For comparison, part (a) of the figure shows the mean photon number distribution in the far field. The numbers associated with the scale in (a) represent the number of photons detected over a resolution area D_R and over a crystal coherence time, which is the mean *photon number per mode*. Both plots have been obtained by filtering the emitted frequencies in a bandwidth $\Delta\lambda=8$ nm wide

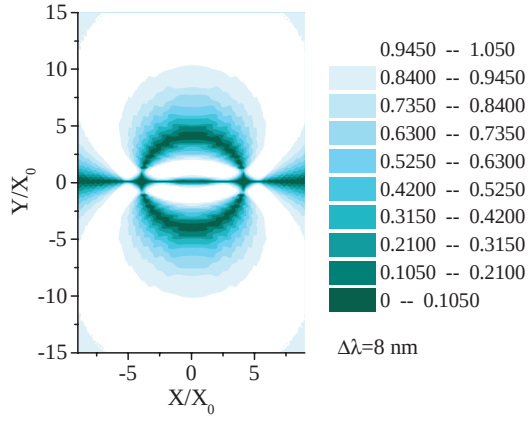

FIG. 5. Degree of polarization of the light down-converted by a BBO crystal. Far-field distribution of $\langle \hat{S}_1(\vec{x})\rangle/\langle \hat{S}_0(\vec{x})\rangle$. Same parameters as in Fig. 4.

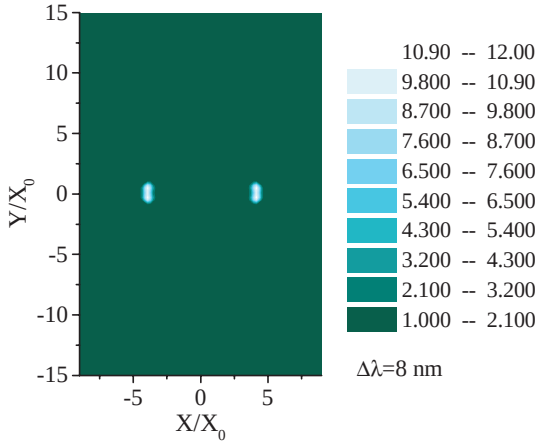

FIG. 6. Noise in the measurement of Stokes parameters of the down-converted light by a BBO crystal. Far-field distribution of $\langle[\delta\hat{S}_2(\vec{x})]^2\rangle/\langle\hat{S}_0(\vec{x})\rangle = \langle[\delta\hat{S}_3(\vec{x})]^2/\langle\hat{S}_0(\vec{x})\rangle$. Same parameters as in Fig. 4.

around the degenerate frequency, by means of a step-function filter. Precisely, we let

$$\hat{A}_i(\vec{x},\Omega)\rightarrow\sqrt{f(\Omega)}\hat{A}_i(\vec{x},\Omega)+\sqrt{1-f(\Omega)}\hat{v}_i(\vec{x},\Omega),\quad i=o,e, \tag{77}$$

where $\hat{v}_i(\vec{x},\Omega)$ are vacuum field operators uncorrelated from the signal and idler fields $\hat{A}_i(\vec{x},\Omega)$, and the filter function $f(\Omega)$ in this case is the step function $f(\Omega)=1$ for $\Omega\epsilon[-\Delta\Omega/2,\Delta\Omega/2]$, $f(\Omega)=0$ elsewhere.

In plot (b) we see clearly two large dark zones, in correspondence of the intersections of the emission cones, where the Stokes operator correlation is almost perfect. Out of these regions, basically no spatial correlation at the quantum level exists for Stokes operators S_2 and S_3.

Remarkably, at the intersection of the two degenerate emission cones, the light is completely unpolarized. Figure 5 shows the distribution of $\langle \hat{S}_1(\vec{x})\rangle/\langle \hat{S}_0(\vec{x})\rangle$ in the transverse far-field plane, showing that it vanishes at the emission ring intersection; recalling that the mean value of $\hat{S}_2$ and $\hat{S}_3$ is zero everywhere, this means a vanishing degree of polarization in these regions. Moreover, in these regions a measurement of Stokes parameters over a single detection pixel is very noisy, as shown in Fig. 6, which plots the distribution of $\langle[\delta\hat{S}_2(\vec{x})]^2\rangle=\langle[\delta\hat{S}_3(\vec{x})]^2\rangle$, scaled to the shot-noise level $\langle\hat{S}_0(\vec{x})\rangle$. In this plot the uniform dark background corresponds to the shot-noise level, while the bright spots correspond to a noise level 10–12 times larger than the shot noise.

Similar results are obtained in any gain regime. In the small gain limit, the noise statistics associated with a measurement over a single pixel becomes essentially Poissonian, but the correlation between Stokes parameters measured from symmetric pixels is basically the same as in the high gain regime. Figure 7 compares the noise in the difference between Stokes parameters measured from symmetric pixels in the small and high gain regimes, plotted as a function of the vertical coordinate y of the signal pixel position. x coordinate is chosen by following the circle of maximum gain for the degenerate frequency (the black curve in the upper half of Fig. 2), so that $y=0$ corresponds to the intersection of the two down-conversion rings. The dashed lines were obtained with $\sigma=0.01$, corresponding to a mean photon number per mode $\approx 10^{-4}$, the solid lines with $\sigma=2$, corresponding to a mean photon number per mode ≈ 15 [see Fig. 4(a)]. In this plot, the two dark lines are, as usual, obtained by filtering the frequencies with a step function ($\Delta\lambda=5$ nm). For comparison, the two light lines show the results obtained by means of a more realistic frequency filter, with a Gaussian profile. Precisely, we take the filter function in Eq. (77) as $f(\Omega)=\exp[-(\Omega^2 4\ln 2)/(\Delta\Omega^2)]$, where $\Delta\Omega$ is the full width at half maximum (FWHM) and corresponds to an interval in wavelengths of 5 nm. In this case, losses introduced by the Gaussian shape of the filter slightly deteriorate the correlation.

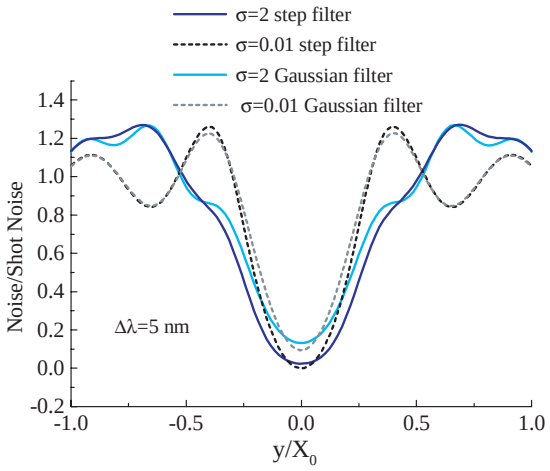

FIG. 7. Noise in the difference between $\hat{S}_2$ ($\hat{S}_3$) measured from symmetric portions of the beam cross section, scaled to the shot-noise level, as a function of the vertical coordinate y along the maximum gain circle for the degenerate frequency. Dashed lines, $\sigma=0.01$; solid lines, $\sigma=2$. Light lines: Gaussian frequency filter of FWHM of 5 nm. Dark lines: step-function filter 5 nm wide.

The results described above were obtained by exploiting a trick commonly used in the experiments performed in the coincidence count regime (for example in the experiment of Ref. [6]), in order to partially compensate for the temporal and spatial walk-off of the down-converted beams. In the regime of single pair production, the ordinary and extraordinary photons can be in principle distinguished because of their different group velocities inside the crystal, and because of their offsets in propagation directions due to walk-off effects inside the crystal. The mere existence of this possibility is detrimental for the entanglement of the state. As it is discussed in detail in Appendix A, in the general case (arbitrary number of down-converted photons), the group-velocity mismatch and the spatial walk-off are responsible for the appearance of a propagation phase factor that lowers the value of the correlation function between Stokes operators measured from symmetric regions. In principle, this problem can be solved by using a very narrow frequency filter, and by performing the measurement over narrow regions centered around the ring intersections. However, this lowers the efficiency of the setup. Another possibility is to insert a second crystal, after the pump beam has been removed, and after the field polarization has been rotated by 90° (see Fig. 3). In this way, the slow and fast waves in the first crystal become the fast and slow waves, respectively, in the second crystal, and the direction of walk-off is reversed. Unlike the low gain regime, the correlation is optimized when the length of this second crystal is chosen as

$$l_c' = l_c \frac{\tanh \sigma}{2\sigma}, \tag{78}$$

where σ is the linear gain parameter, proportional to the pump amplitude and to the first-crystal length (see Appendix A). The fact that the optimal length of the compensation crystal decreases with increasing gain can be understood as following [25,26]: in the low gain regime (limit $\sigma \to 0$), the photon pair can be produced at any point along the crystal length with uniform probability, so that the average temporal delays of the two photons due to the group-velocity mismatch are those corresponding to half of the crystal length, and best compensation is achieved for $l_c' = l_c/2$. In the large gain regime, more and more photon pairs are produced towards the end of the crystal (the number of down-converted photons increases exponentially with the crystal length), so that walk-off effects are best compensated by a shorter crystal, whose length is given by formula (78).

When this kind of optimization is not possible, our calculations show that similar results can be obtained by a narrowband temporal and spatial filtering, and/or by using crystals that exhibit a smaller amount of walk-off. Figure 8 details the role of the compensation crystal. It plots the noise in the difference between Stokes parameters measured from symmetric pixels as a function of the vertical coordinate y along the circle corresponding to the maximum gain at the degenerate frequency.

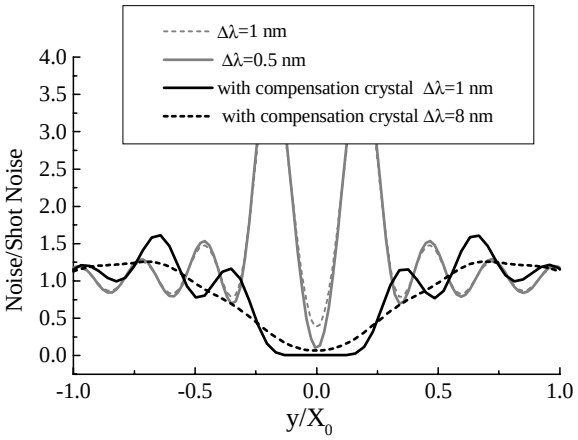

FIG. 8. Effect of the compensation crystal. Noise in the difference between $\hat{S}_2$ measured from symmetric pixels, scaled to the shot-noise level. y is the far-field vertical position along the maximum gain circle. Gray lines: without compensation crystal, dashed gray line $\Delta\lambda = 1$ nm, solid gray line $\Delta\lambda = 0.5$ nm. Black lines: with optimal compensation crystal, solid black line $\Delta\lambda = 1$ nm, dashed black line $\Delta\lambda = 8$ nm.

2. Broadband frequency filtering results

The results described in Sec. III D 1 were obtained by using relatively narrow frequency filters (5–8 nm). Remarkably, when a broader frequency filter is employed, the regions where Stokes parameters are correlated stretch to form a ring-shaped region around the pump direction (see Fig. 9). This kind of shape can be understood by considering the geometry of the down-conversion cones emitted at the various frequencies by a BBO crystal. Figure 10 is a polar plot of the phase-matching curves (geometrical loci of the phase-matched modes), with θ being the polar angle from the pump direction of propagation (z axis) and ϕ the azimuthal angle around z. In this plot the same color identifies the same emission wavelength; dark/light thick curves correspond to two conjugate wavelengths, while the thin black curves are the two emission cones at the degenerate wavelength. The signal (ordinary) wave emission curves are those in the upper half of the plot. When considering the intersection points of a dark circle with a light circle, which correspond to two conjugate wavelengths, we cannot expect any kind of entanglement, since photons arriving in these positions are clearly distinguishable by their different frequencies. Let us consider, instead, one of the intersections of the two light curves (e.g., the one pointed by the arrow in the plot). Here ordinary and extraordinary photons arrive with identical probability, and have the same wavelength. As a consequence, the photon polarization is undetermined, and the light is completely unpolarized. However, each time an ordinary (extraordinary) photon arrives at this position, an extraordinary (ordinary) photon, at the conjugate wavelength, will be found at the symmetric position. This corresponds to the intersection of the two dark curves, indicated in the plot by the second arrow. Hence, when considering photodetection from the two regions indicated by the arrows in the plot we can expect a high degree of polarization entanglement. The same reasoning can be made for any intersection of circles corresponding

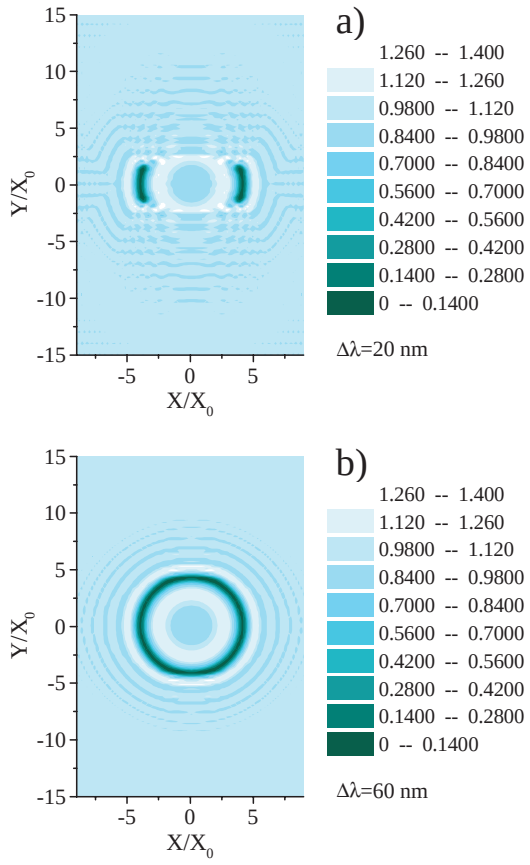

FIG. 9. Broadband frequency filtering. Distribution of the noise in the difference between $\hat{S}_2$ ($\hat{S}_3$) measured from symmetric portions of the beam cross section, scaled to the shot-noise level. In part (a) a frequency filter $\Delta\lambda = 20$ nm wide centered around the degenerate frequency is used; in (b) $\Delta\lambda = 60$ nm.

to the same wavelength (light with light, dark with dark, and thin black with thin black). By connecting all these points together, we can for example recognize the geometrical shape of the dark regions in Fig. 9(a), where a high degree of correlation in all the Stokes parameters exists. By including more frequencies, the ring-shaped region of Fig. 9(b) shows up.

From the mathematical point of view, the form of the region where Stokes parameters are quantum correlated is given by the solution of the equation

$$\Delta(\vec{q},\Omega) = \Delta(-\vec{q},-\Omega) = 0 \tag{79}$$

with $\vec{x} = 2\pi\vec{q}/(\lambda f)$. By introducing the explicit form of the phase-mismatch function (24), Eq. (79) is the equation of an ellipse (with a small eccentricity) centered around the origin, that is, the best correlated modes form a slightly asymmetric cone around the pump direction.

IV. POLARIZATION CORRELATION: QUANTUM-STATE FORMALISM

This section is devoted to the discussion of the problem in terms of an equivalent quantum state formalism. Our aim is,

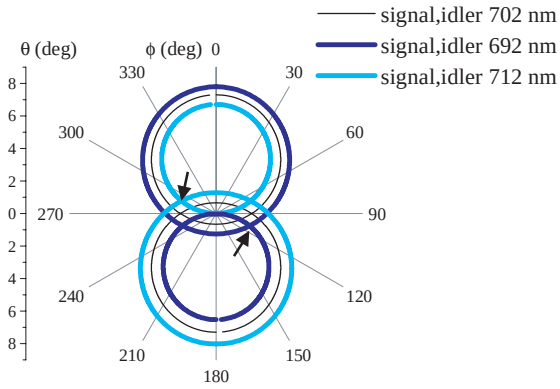

FIG. 10. Polar plot of phase-matching curves in a 2-mm BBO crystal cut at 49.6°. θ is the polar angle from the pump direction of propagation; ϕ is the azimuthal angle around the pump. Black thin curves: $\lambda_{signal} = \lambda_{idler} = 702$ nm. Dark thick curves: $\lambda_{signal} = \lambda_{idler} = 692$ nm. Light thick curves: $\lambda_{signal} = \lambda_{idler} = 712.29$ nm. Signal (ordinary) curves are in the upper half of the plot, idler (extraordinary) in the lower half.

on the one side, to give an alternative and instructive point of view on the problem, which can be compared with already existing quantum-state description of the problem (see, e.g., Ref. [11]). On the other side, we think that this section will show how the quantum-field formalism developed in the first part of this paper is more powerful and straightforward, in terms of calculation efforts, than the commonly used quantum-state formalism, at least for this kind of multimode problems.

Equation (11) defines a linear transformation acting on field operators, which maps field operators at the entrance face of the crystal into those at the output face. An equivalent transformation, acting on the quantum state of the signal/idler fields at the crystal input and mapping it into the state at the crystal output, is derived in detail in Appendix B. As described in this appendix, in order to avoid formal difficulties coming from a continuum of modes, we have introduced a quantization box both in the transverse spatial domain and in the temporal domain, so that the continuum of spatiotemporal modes $\vec{q},\Omega$ is replaced by a discrete set of modes.

When at the input of the parametric crystal there is the vacuum state for both signal and idler fields,

$$|\psi\rangle_{in} = |\mathrm{vac}\rangle = \prod_{\vec{q},\Omega} |0;-\vec{q},-\Omega\rangle_o |0;\vec{q},\Omega\rangle_e , \tag{80}$$

we find that the output state takes the form

$$|\psi\rangle_{out} = \prod_{\vec{q},\Omega} \left\{ \sum_{n=0}^{\infty} c_n(\vec{q},\Omega) |n;\vec{q},\Omega\rangle_o |n;-\vec{q},-\Omega\rangle_e \right\}, \tag{81}$$

$$c_n(\vec{q},\Omega) = \frac{1}{\cosh r(\vec{q},\Omega)} [\tanh r(\vec{q},\Omega)]^n e^{2in\psi(\vec{q},\Omega)}$$

$$= \frac{[U_o(\vec{q},\Omega) V_e(-\vec{q},-\Omega)]^n}{|U_o(\vec{q},\Omega)|^{2n+1}}, \tag{82}$$

where the notation $|n;\vec{q},\Omega\rangle_{o/e}$ indicates the Fock state with n photons in mode $(\vec{q},\Omega)$ of the ordinary/extraordinary polarized beam. Here the functions U_o, V_e are the coefficients of the operator transformation (11), and functions r and ψ are defined by Eqs. (17) and (18) together with Eqs. (19) and (20).

State (82) is clearly entangled (nonfactorizable) with respect to the ordinary and extraordinary polarized beam components.

Let us focus on two conjugate modes $\vec{q},\Omega$ and $-\vec{q},-\Omega$ for both the ordinary and extraordinary field components. These can be for example observed by using a narrow filter around the degenerate frequency $\Omega=0$ and collecting light from two diaphragms placed around two symmetric regions in the far-field zone. For brevity of notation, let us label these modes with the three-dimensional vectors $\vec{\xi}=(q_x,q_y,\Omega)$, $-\vec{\xi}=(-q_x,-q_y,-\Omega)$. When restricted to these modes, the state takes the form

$$|\psi\rangle_{out}^{\vec{\xi}}=\left\{\sum_n c_n(\vec{\xi})|n;\vec{\xi}\rangle_o|n;-\vec{\xi}\rangle_e\right\}\times\left\{\sum_{n'} c_{n'}(-\vec{\xi})|n';-\vec{\xi}\rangle_o|n';\vec{\xi}\rangle_e\right\} \tag{83}$$

$$=\sum_{N=0}^{\infty}|\phi\rangle_N^{\vec{\xi}}, \tag{84}$$

$$|\phi\rangle_N^{\vec{\xi}}=\sum_{m=0}^{N}\gamma_{N,m}(\vec{\xi})|m;\vec{\xi}\rangle_o|N-m;\vec{\xi}\rangle_e|N-m;-\vec{\xi}\rangle_o\times|m;-\vec{\xi}\rangle_e, \tag{85}$$

where the last two lines have been obtained by changing the dummy summation variables n,n' into $m=n$, $N=n+n'$. The state can be represented as a superposition of states with a fixed total number of photons N. In each N-photon state described by Eq. (85),

$$\gamma_{N,m}(\vec{\xi})=c_m(\vec{\xi})c_{N-m}(-\vec{\xi})=\frac{[\tanh r(\vec{\xi})]^m[\tanh r(-\vec{\xi})]^{N-m}}{\cosh r(\vec{\xi})\cosh r(-\vec{\xi})}\times e^{2iN\psi(-\vec{\xi})}e^{2im[\psi(\vec{\xi})-\psi(-\vec{\xi})]} \tag{86}$$

represents the probability *amplitude* of finding m ordinary photons, $N-m$ extraordinary photons in mode $\vec{\xi}$, and $N-m$ ordinary photons, m extraordinary photons in the conjugate mode $-\vec{\xi}$. The description of the state given by Eqs. (83)–(85) is a generalization of that derived in, e.g., Ref. [11]. The main improvement is that our description includes the effects of the spatial and the temporal walk-off, and allows the quantitative evaluation of all the quantities of interest by using the parameters of a real crystal. Remarkably, when the spatial and the temporal walk-off are not taken into account, the symmetry $(\vec{q},\Omega)\rightarrow(-\vec{q},-\Omega)$ holds. In this case, in Eq. (86) we would have $r(-\vec{\xi})=r(\vec{\xi})$ and $\psi(-\vec{\xi})=\psi(\vec{\xi})$, and all the coefficients $\gamma_{N,m}(\vec{\xi})$ would be identical for a given N, so that all the terms in expansion (85) would have the same weight, thus leading to a "*maximally entangled state for polarization*" [11].

Coming to Stokes parameter correlation we notice the following property of the state:

$$[\hat{A}_o^\dagger(\vec{\xi})\hat{A}_o(\vec{\xi})-\hat{A}_e^\dagger(\vec{\xi})\hat{A}_e(\vec{\xi})]|\phi\rangle_N^{\vec{\xi}}=\sum_{m=0}^{N}c_m(\vec{\xi})c_{N-m}(-\xi)(2m-N)|m;\vec{\xi}\rangle_o|N-m;\vec{\xi}\rangle_e\times|N-m;-\vec{\xi}\rangle_o|m;-\vec{\xi}\rangle_e \tag{87}$$

$$=-[\hat{A}_o^\dagger(-\vec{\xi})\hat{A}_o(-\vec{\xi})-\hat{A}_e^\dagger(-\vec{\xi})\hat{A}_e(-\vec{\xi})]|\phi\rangle_N^{\vec{\xi}}. \tag{88}$$

By recalling the definition of the Stokes operator densities given by Eqs. (38)–(40), $\hat{\sigma}_1(\vec{\xi})=\hat{A}_o^\dagger(\vec{\xi})\hat{A}_o(\vec{\xi})-\hat{A}_e^\dagger(\vec{\xi})\hat{A}_e(\vec{\xi})$, $\hat{\sigma}_2(\vec{\xi})=\hat{A}_o^\dagger(\vec{\xi})\hat{A}_e(\vec{\xi})+\hat{A}_e^\dagger(\vec{\xi})\hat{A}_o(\vec{\xi})$, and $\hat{\sigma}_3(\vec{\xi})=-i[\hat{A}_o^\dagger(\vec{\xi})\hat{A}_e(\vec{\xi})-\hat{A}_e^\dagger(\vec{\xi})\hat{A}_o(\vec{\xi})]$, we can hence conclude that the state is an eigenstate of $\hat{\sigma}_1(\vec{\xi})+\hat{\sigma}_1(-\vec{\xi})$ with zero eigenvalue. On the other side, we have

$$\hat{A}_o^\dagger(\vec{\xi})\hat{A}_e(\vec{\xi})|\phi\rangle_N^{\vec{\xi}}=\sum_{m=0}^{N-1}c_m(\vec{\xi})c_{N-m}(-\xi)\times\sqrt{(m+1)(N-m)}|m+1;\vec{\xi}\rangle_o\times|N-m-1;\vec{\xi}\rangle_e|N-m;-\vec{\xi}\rangle_o|m;-\vec{\xi}\rangle_e, \tag{89}$$

$$\hat{A}_o^\dagger(-\vec{\xi})\hat{A}_e(-\vec{\xi})|\phi\rangle_N^{\vec{\xi}}=\sum_{m=1}^{N}c_m(\vec{\xi})c_{N-m}(-\xi)\times\sqrt{m(N-m+1)}|m;\vec{\xi}\rangle_o|N-m;\vec{\xi}\rangle_e\times|N-m+1;-\vec{\xi}\rangle_o|m-1;-\vec{\xi}\rangle_e \tag{90}$$

$$=\sum_{l=0}^{N-1}c_{l+1}(\vec{\xi})c_{N-l-1}(-\xi)\times\sqrt{(l+1)(N-l)}|l+1;\vec{\xi}\rangle_o\times|N-l-1;\vec{\xi}\rangle_e|N-l;-\vec{\xi}\rangle_o|l;-\vec{\xi}\rangle_e, \tag{91}$$

where the last line has been obtained by introducing the summation index $l=m-1$. This implies that the equation

$$[\hat{A}_o^\dagger(\vec{\xi})\hat{A}_e(\vec{\xi})-\hat{A}_o^\dagger(-\vec{\xi})\hat{A}_e(-\vec{\xi})]|\psi\rangle_{out}^{\vec{\xi}}=0 \tag{92}$$

is verified if and only if

$$c_m(\vec{\xi})c_{N-m}(-\vec{\xi}) = c_{m+1}(\vec{\xi})c_{N-m-1}(-\vec{\xi}) \tag{93}$$

for all $N=0,+\infty$ and $m=0,N-1$.

Similar considerations for the Hermitian conjugate operator $\hat{A}_e^\dagger(\vec{\xi})\hat{A}_o(\vec{\xi}) - \hat{A}_e^\dagger(-\vec{\xi})\hat{A}_o(-\vec{\xi})$ lead to the equivalent condition

$$c_m(\vec{\xi})c_{N-m}(-\vec{\xi}) = c_{m-1}(\vec{\xi})c_{N-m+1}(-\vec{\xi}) \tag{94}$$

for all $N=0,+\infty$ and $m=1,N$.

Hence, the state is also an eigenstate of both $\hat{\sigma}_2(\vec{\xi}) - \hat{\sigma}_2(-\vec{\xi})$ and $\hat{\sigma}_3(\vec{\xi}) - \hat{\sigma}_3(-\vec{\xi})$, with zero eigenvalue, if and only if conditions (93) and (94) are satisfied. These conditions amount to requiring that all the coefficients in the expansion of the N-photon state (85) are identical, and that the N-photon state is a superposition with equal probability amplitude of all the possible partitions in m ordinary and $N-m$ extraordinary photons ($m=0,N$) in mode $\vec{\xi}$, with $N-m$ ordinary and m extraordinary photons in the conjugate mode $-\vec{\xi}$. This is the mathematical equivalent of the commonly used statement ''ordinary and extraordinary photons in mode $\vec{\xi}$ are not distinguishable, but each time we have m ordinary and $N-m$ extraordinary photon in mode $\vec{\xi}$, there are $N-m$ ordinary and m extraordinary photons in mode $-\vec{\xi}$.'' For modes having a nonvanishing parametric gain conditions (93) and (94) amount to requiring

$$\tanh r(\vec{\xi})e^{2i\psi(\vec{\xi})} = \tanh r(-\vec{\xi})e^{2i\psi(-\vec{\xi})}, \tag{95}$$

a condition that is satisfied only in the presence of the symmetry $\Delta(\vec{q},\Omega)=\Delta(-\vec{q},-\Omega)$. This in turn implies the absence of spatial walk-off between the two waves (i.e., the two modes correspond to the intersection of the down-conversion cones) and the absence of temporal walk-off (use of a narrow frequency filter and/or compensation by means of a second crystal).

Formula (95) can be also written as

$$U(\vec{\xi})V^*(-\vec{\xi}) = U(-\vec{\xi})V^*(\vec{\xi}). \tag{96}$$

By comparing with Eq. (73), we notice that this is the condition that ensures that the correlation between Stokes parameter measured from symmetric pixels calculated in Sec. III D reaches its maximum value. Hence, in the framework of the quantum-state formalism, we start to recover the same results of Sec. III B, as it obviously must be. One could proceed further on, and derive quantitative results for the correlation, as those shown by Figs. 4–9, but at this point it should be rather clear (and for sure we are not the first ones to notice this) how the quantum-state formalism, although instructive, is cumbersome and not transparent in comparison with the quantum-field formalism.

V. CONCLUSIONS

In conclusion, we have shown that the polarization entanglement of photon pairs emitted in parametric down-conversion survives in high gain regimes, where the number of converted photons can be rather large. In this case, it takes the form of nonclassical spatial correlations of *all* light Stokes operators associated with polarization degrees of freedom. We have shown that in the regions where the two rings intersect (in a ring-shaped region around the pump direction when a broad frequency filter is employed) all the Stokes operators are highly correlated at a quantum level, realizing in this way a macroscopic polarization entanglement. Although Stokes parameters are extremely noisy and the state is unpolarized, measurement of a Stokes parameter *in any polarization basis* in one far-field region determines the Stokes parameter collected from the symmetric region, within an uncertainty much below the standard quantum limit.

We call this situation ''polarization entanglement'' because, on the one side, the quantum state derived in Sec. IV is entangled with respect to polarization degrees of freedom, and, on the other, because in our description there is no gap in the passage from the regime of single photon pair detection, where the polarization entanglement is a widely accepted concept, to the regime of multiple pair production. However, we want to remark that for spontaneous parametric down-conversion there is no way, to our knowledge, to derive a sufficient criterion for inseparability based on the degree of correlation of the Stokes operators, as that derived in Ref. [24] and generalized in Ref. [3]. This depends on the fact that the average values of commutators (and anticommutators) of Stokes operators are in this system intrinsically state dependent, at difference to what happens in the experiment performed in Ref. [3], where bright entangled beams were used. Further discussion about this important point is postponed to future investigations, which are outside the scope of this paper.

We have developed a multimode model for spontaneous parametric down-conversion, both within the framework of quantum-field formalism and quantum-state formalism. They are valid in any gain regime, from the single-photon pair production to the high gain regime where the number of down-converted photons can be rather large. The model allows quantitative estimations of all the quantities of interest, by using empirical parameters of real crystals. We hope that this description can be a useful tool for experimentalists working in this field.

Quite interesting, and to our knowledge completely novel, are the results concerning the correlation of Stokes parameters observed by using a broad frequency filter, described in Sec. III D 2. They basically show how by increasing the number of temporal degrees of freedom in play, the number of spatial degrees of freedom which are simultaneously entangled increases, so that the two isolated correlated spots in Fig. 4 become the ring-shaped region of Fig. 9, where many symmetric spots are correlated in pairs.

We believe that this form of entanglement, with its increased complexity in terms of degrees of freedom (photon number, polarization, temporal, and spatial degrees of freedom) can be quite promising for new quantum information schemes.

ACKNOWLEDGMENTS

This work was carried out in the framework of the EU project QUANTIM (Quantum Imaging). Two of us (R.Z. and

M.S.M.) acknowledge financial support from the Spanish MCyT Project No. BFM2000-1108.

APPENDIX A

In this appendix we calculate the phase shift induced by the propagation of the down-converted fields through a compensation crystal and evaluate the length of this second crystal necessary for optimal walk-off compensation. As shown by the scheme of Fig. 3, we assume that after producing down-conversion in a first crystal (BBO1), the pump beam is eliminated. The polarizations of the down-converted beams are then rotated by 90°, and they pass through a second crystal (BBO2) of length l_c', identical to the first one.

In the region between the second crystal and the lens L the ordinary/extraordinary field operators can be written as

$$\hat{A}_o(\vec{q},\Omega,z)=\hat{A}_e^{out}(\vec{q},\Omega)\exp[ik_{oz}(\vec{q},\Omega)l_c'] \times\exp[i\phi_{vac}(z-l_c')], \tag{A1}$$

$$\hat{A}_e(\vec{q},\Omega,z)=\hat{A}_o^{out}(\vec{q},\Omega)\exp[ik_{ez}(\vec{q},\Omega)l_c'] \times\exp[i\phi_{vac}(z-l_c')]. \tag{A2}$$

The first phase shift accounts for propagation inside the compensation crystal. Here $k_{oz}(\vec{q},\Omega)$, $k_{ez}(\vec{q},\Omega)$ are the projections along z axis of the ordinary/extraordinary wave vectors inside the crystal, whose explicit expressions depend on the linear properties of the crystal as described by Eq. (23). The second phase shift accounts for paraxial propagation in vacuum $\phi_{vac}(z)=(k-q^2/2k)z$, $k=2\pi/\lambda$.

In the far-field plane, all the results described in Secs. III C and III D remain unchanged provided that one makes the following substitutions:

$$\mathcal{U}_o(\vec{x},\Omega)\to U_e(\vec{q},\Omega)\exp[ik_{oz}(\vec{q},\Omega)l_c']|_{q=\vec{x}(2\pi/\lambda f)}, \tag{A3}$$

$$\mathcal{V}_o(\vec{x},\Omega)\to V_e(\vec{q},\Omega)\exp[ik_{oz}(\vec{q},\Omega)l_c']|_{q=\vec{x}(2\pi/\lambda f)}, \tag{A4}$$

$$\mathcal{U}_e(\vec{x},\Omega)\to U_o(\vec{q},\Omega)\exp[ik_{ez}(\vec{q},\Omega)l_c']|_{q=\vec{x}(2\pi/\lambda f)}, \tag{A5}$$

$$\mathcal{V}_e(\vec{x},\Omega)\to V_o(\vec{q},\Omega)\exp[ik_{ez}(\vec{q},\Omega)l_c']|_{\vec{q}=\vec{x}(2\pi/\lambda f)}, \tag{A6}$$

where global phase factors have been omitted, since they do not affect the results.

This transformation leaves unchanged all the results described in Sec. III C (noise and correlation for measurements of Stokes operators 0 and 1). For the second and third Stokes parameters (Sec. III D), while the transformation does not affect the amount of noise of the measurement, given by Eqs. (69) and (71), it does affect the correlation between measurements from symmetric pixels [Eqs. (70) and (72)]:

$$H_2(\vec{x},0)\to\int\frac{d\omega}{2\pi}2\,\mathrm{Re}\{\mathcal{U}^*(-\vec{x},-\omega)\mathcal{U}(\vec{x},\omega)\mathcal{V}^*(-\vec{x},-\omega) \times\mathcal{V}(\vec{x},\omega)e^{i\phi_c(\vec{x},\Omega)}\}, \tag{A7}$$

$$\phi_c(\vec{x},\Omega)=[k_{ez}(\vec{q},\Omega)+k_{oz}(-\vec{q},-\Omega)-k_{oz}(\vec{q},\Omega) -k_{ez}(-\vec{q},-\Omega)]l_c'|_{\vec{q}=\vec{x}(2\pi/\lambda f)} \tag{A8}$$

$$=[\Delta(-\vec{q},-\Omega)-\Delta(\vec{q},\Omega)]\frac{l_c'}{l_c}\bigg|_{\vec{q}=\vec{x}(2\pi/\lambda f)}. \tag{A9}$$

On the other side, by using the explicit expression of the gain functions in Eqs. (19) and (20), we have

$$\arg\{\mathcal{U}^*(-\vec{x},-\omega)\mathcal{U}(\vec{x},\omega)\mathcal{V}^*(-\vec{x},-\omega)\mathcal{V}(\vec{x},\omega)\} =2\psi(\vec{q},\Omega)-2\psi(-q,-\Omega)|_{\vec{q}=\vec{x}(2\pi/\lambda f)} \tag{A10}$$

with

$$2\psi(\vec{q},\Omega)=\tan^{-1}\left\{\Delta(\vec{q},\Omega)\frac{\tanh\Gamma(\vec{q},\Omega)}{2\Gamma(\vec{q},\Omega)}\right\} \tag{A11}$$

$$\approx\Delta(\vec{q},\Omega)\frac{\tanh\sigma}{2\sigma}. \tag{A12}$$

The last line has been obtained by taking the limit $\Delta(\vec{q},\Omega)\ll 1$; this is meaningful since the most important contribution to the correlation function is given by phase-matched modes. The phase factor (A10) can be partially compensated by the phase shift induced by propagation in the second crystal (A9). Best compensation is achieved for

$$\frac{l_c'}{l_c}=\frac{\tanh\sigma}{2\sigma}. \tag{A13}$$

In this condition the value of the correlation between measurements from symmetric pixel (the value of the function H_2) is maximized by the presence of a compensation crystal.

APPENDIX B

Equation (11) defines a linear transformation acting on field operators, which maps field operators at the entrance face of the crystal into those at the output face. The aim of this appendix is to find an equivalent transformation acting on the quantum state of the signal/idler fields at the crystal input and mapping it into the state at the crystal output.

In order to avoid formal difficulties coming from a continuum of modes, we introduce a quantization box of side b in the transverse plane, with periodic boundary conditions. In this way the continuum of wave vectors $\vec{q}$ is replaced by a set of discrete wave vectors $q_{\vec{l}}=(l_x\vec{u}_x+l_y\vec{u}_y)(2\pi/b)$, $l_x,l_y=0,\pm1,\pm2,\ldots$. In the same way, we introduce a quantization box in the time domain of length T, with periodic boundaries, so that we need to consider only a discrete set of temporal frequencies $\Omega_p=p(2\pi/T)$, $p=0,\pm1,\ldots$. The free field commutation relations (12) are thus replaced by their discrete version $[\hat{A}_i(\vec{q}_{\vec{l}},\Omega_p),\hat{A}_j^\dagger(\vec{q}_{\vec{m}},\Omega_s)] =\delta_{i,j}\delta_{l_x,m_x}\delta_{l_y,m_y}\delta_{n,s}$, $i,j=0,e$.

For brevity of notation, in the following we shall indicate

the spatiotemporal mode $\vec{q}_{\vec{l}},\Omega_p$ with the three-dimensional vector $\vec{\xi}$, and we shall not write explicitly the modal indices.

The input/output transformation (11) can be written in an equivalent way as

$$\hat{A}_i(\vec{\xi})=\hat{R}^\dagger \hat{A}_i^{in}(\vec{\xi})\hat{R}, \tag{B1}$$

with

$$\hat{R}=\hat{R}_0\hat{R}_1\hat{R}_2, \tag{B2}$$

and

$$\hat{R}_0=\exp\left\{ i\sum_{\vec{\xi}} [\psi(\vec{\xi})+\varphi(\vec{\xi})]\hat{A}_o^\dagger(\vec{\xi})\hat{A}_o(\vec{\xi}) + [\psi(\vec{\xi})-\varphi(\vec{\xi})]\hat{A}_e^\dagger(-\vec{\xi})\hat{A}_e(-\vec{\xi})\right\}, \tag{B3}$$

$$\hat{R}_1=\exp\left\{ \sum_{\vec{\xi}} r(\vec{\xi})[\hat{A}_o^\dagger(\vec{\xi})\hat{A}_e^\dagger(-\vec{\xi})-\hat{A}_o(\vec{\xi})\hat{A}_e(-\vec{\xi})]\right\}, \tag{B4}$$

$$\hat{R}_2=\exp\left\{ i\sum_{\vec{\xi}} \theta(\vec{\xi})[\hat{A}_o^\dagger(\vec{\xi})\hat{A}_o(\vec{\xi})+\hat{A}_e^\dagger(-\vec{\xi})\hat{A}_e(-\vec{\xi})]\right\} \tag{B5}$$

with functions $\psi(\vec{\xi}),\varphi(\vec{\xi}),r(\vec{\xi}),\theta(\vec{\xi})$ defined by Eqs. (17) and (18), together with Eqs. (19)–(21).

In order to demonstrate ansatz (B1), we first notice that the action of operators $\hat{R}_0$ and $\hat{R}_2$ on field operators corresponds to phase rotations. For any boson operator $\hat{c}$, for which $[\hat{c},\hat{c}^\dagger]=1$, we have

$$e^{-is\hat{c}^\dagger\hat{c}}\hat{c}e^{is\hat{c}^\dagger\hat{c}}=e^{is}\hat{c}. \tag{B6}$$

As a consequence,

$$\hat{R}_0^\dagger\hat{A}_o(\vec{\xi})\hat{R}_0=\hat{A}_o(\vec{\xi})e^{i[\psi(\vec{\xi})+\varphi(\vec{\xi})]}, \tag{B7}$$

$$\hat{R}_0^\dagger\hat{A}_e(\vec{\xi})\hat{R}_0=\hat{A}_e(\vec{\xi})e^{i[\psi(-\vec{\xi})-\varphi(-\vec{\xi})]}. \tag{B8}$$

Operator $\hat{R}_1$ is the product of an infinity of two-mode squeezing operators, each of them acting on the couple of modes $(\vec{\xi})$ in the signal beam and $(-\vec{\xi})$ in the idler beam. For any couple of independent boson operators $\hat{c}_1,\hat{c}_2$, and for r real, the identity

$$e^{-r[\hat{c}_1^\dagger\hat{c}_2^\dagger-\hat{c}_1\hat{c}_2]}\hat{c}_1e^{+r[\hat{c}_1^\dagger\hat{c}_2^\dagger-\hat{c}_1\hat{c}_2]}=\hat{c}_1\cosh r+\hat{c}_2^\dagger\sinh r \tag{B9}$$

holds.

Hence, letting $\hat{c}_1\to\hat{A}_o(\vec{\xi})$, $\hat{c}_2\to\hat{A}_e(-\vec{\xi})$, we have

$$\hat{R}_1^\dagger\hat{A}_o(\vec{\xi})\hat{R}_1=\hat{A}_o(\vec{\xi})\cosh r(\vec{\xi})+\hat{A}_e^\dagger(-\vec{\xi})\sinh r(\vec{\xi}), \tag{B10}$$

$$\hat{R}_1^\dagger\hat{A}_e(\vec{\xi})\hat{R}_1=\hat{A}_e(\vec{\xi})\cosh r(-\vec{\xi})+\hat{A}_o^\dagger(-\vec{\xi})\sinh r(-\vec{\xi}). \tag{B11}$$

Finally, by letting also the operator $\hat{R}_2$ act as

$$\hat{R}_2^\dagger\hat{R}_1^\dagger\hat{R}_0^\dagger\hat{A}_o(\vec{\xi})\hat{R}_0\hat{R}_1\hat{R}_2=e^{i[\psi(\vec{\xi})+\varphi(\vec{\xi})]}\{\hat{A}_o(\vec{\xi})\cosh r(\vec{\xi})e^{i\theta(\vec{\xi})} +\hat{A}_e^\dagger(-\vec{\xi})\sinh r(\vec{\xi})e^{-i\theta(\vec{\xi})}\} \tag{B12}$$

$$=e^{i\varphi(\vec{\xi})}\{\hat{A}_o(\vec{\xi})U(\vec{\xi}) +\hat{A}_e^\dagger(-\vec{\xi})V(\vec{\xi})\}, \tag{B13}$$

where in passing from the first to the second line we used relation (18), which is a consequence of the unitarity of transformation (11). Moreover, we have

$$\hat{R}_2^\dagger\hat{R}_1^\dagger\hat{R}_0^\dagger\hat{A}_e(\vec{\xi})\hat{R}_0\hat{R}_1\hat{R}_2 =e^{i[\psi(-\vec{\xi})-\varphi(-\vec{\xi})]}\{\hat{A}_e(\vec{\xi})\cosh r(-\vec{\xi})e^{i\theta(-\vec{\xi})}+\hat{A}_o^\dagger(-\vec{\xi}) \times\sinh r(-\vec{\xi})e^{-i\theta(-\vec{\xi})}\} \tag{B14}$$

$$=e^{-i\varphi(-\vec{\xi})}\{\hat{A}_e(\vec{\xi})U(-\vec{\xi})+\hat{A}_o^\dagger(-\vec{\xi})V(-\vec{\xi})\}. \tag{B15}$$

Finally, taking into account relation (17), which is again a consequence of the unitarity of transformation (11), we recover the input/output transformation (11).

Any quantum-mechanical expectation value of the output operators (mean values, correlation functions, etc.) taken on the input state is equivalent to the quantum-mechanical expectation value of the input operators taken on the transformed state:

$$|\psi\rangle_{out}=\hat{R}|\psi\rangle_{in}. \tag{B16}$$

In the following we shall derive the form of the output state, when at the input of the parametric crystal there is the vacuum state for both signal and idler fields:

$$|\psi\rangle_{in}=|\mathrm{vac}\rangle=\prod_{\vec{\xi}}|0;\vec{\xi}\rangle_o|0;-\vec{\xi}\rangle_e, \tag{B17}$$

where the notation $|n;\vec{\xi}\rangle_{o/e}$ indicates the Fock state with n photons in mode $(\vec{\xi})$ of the ordinary/extraordinary polarized beam.

First of all we notice that the operator $\hat{R}_2$ has no effect on the vacuum state, corresponding to a phase rotation of the vacuum. For what concerns operator $\hat{R}_1$, by using proper operator ordering techniques (see, e.g., Ref. [27]) p. 75), it can be recasted in the following form (*disentangling theorem*):

$$\hat{R}_1=\prod_{\vec{\xi}}\{e^{G(\vec{\xi})\hat{A}_o^\dagger(\vec{\xi})\hat{A}_e^\dagger(-\vec{\xi})}e^{-g(\vec{\xi})[\hat{A}_o^\dagger(\vec{\xi})\hat{A}_o(\vec{\xi})+\hat{A}_e^\dagger(-\vec{\xi})\hat{A}_e(-\vec{\xi})+1]} \times e^{-G(\vec{\xi})\hat{A}_o(\vec{\xi})\hat{A}_e(-\vec{\xi})}\}, \tag{B18}$$

$$G(\vec{\xi}) = \tanh[r(\vec{\xi})], \tag{B19}$$

$$g(\vec{\xi}) = \ln\{\cosh[r(\vec{\xi})]\}. \tag{B20}$$

By letting this operator acting on the vacuum state

$$\hat{R}_1|\mathrm{vac}\rangle = \prod_{\vec{\xi}} \frac{1}{\cosh[r(\vec{\xi})]} \sum_{n=0}^{\infty} [\tanh r(\vec{\xi})]^n |n;\vec{\xi}\rangle_o |n;-\vec{\xi}\rangle_e, \tag{B21}$$

where the usual expansion of the exponential operator $\exp \hat{M} = \Sigma_{n=0}^{\infty} \hat{M}^n/n!$ has been used, together with the standard action of boson creation operators on Fock states. Finally, by adding the action of operator $\hat{R}_0$,

$$\hat{R}_0\hat{R}_1|\mathrm{vac}\rangle = \prod_{\vec{\xi}} \frac{1}{\cosh[r(\vec{\xi})]} \sum_{n} [\tanh r(\vec{\xi})]^n e^{2in\psi(\vec{\xi})} \times |n;\vec{\xi}\rangle_o |n;-\vec{\xi}\rangle_e, \tag{B22}$$

the output state can be written in the form

$$|\psi\rangle_{out} = \prod_{\vec{\xi}} \left\{ \sum_n c_n(\vec{\xi}) |n;\vec{\xi}\rangle_o |n;-\vec{\xi}\rangle_e \right\}, \tag{B23}$$

$$c_n(\vec{\xi}) = \frac{1}{\cosh r(\vec{\xi})} [\tanh r(\vec{\xi})]^n e^{2in\psi(\vec{\xi})} = \frac{[U_o(\vec{\xi}) V_e(-\vec{\xi})]^n}{|U_o(\vec{\xi})|^{2n+1}}. \tag{B24}$$

[1] W.P. Bowen, R. Schnabel, H-A. Bachor, and P.K. Lam, Phys. Rev. Lett. **88**, 093601 (2002).

[2] N. Korolkova, G. Leuchs, R. Loudon, T.C. Ralph, and C. Silberhorn, Phys. Rev. A **65**, 052306 (2002); e-print quant-ph/0108098.

[3] W.P. Bowen, N. Treps, R. Schnabel, and P.K. Lam, Phys. Rev. Lett. **89**, 253601 (2002).

[4] R. Schnabel, W.P. Bowen, N. Treps, T.C. Ralph, H-A. Bachor, and P.K. Lam, Phys. Rev. A **67**, 012316 (2003).

[5] J. Hald, J.L. Srensen, C. Schori, and E.S. Polzik, Phys. Rev. Lett. **83**, 1319 (1999).

[6] P.G. Kwiat, K. Mattle, H. Weinfurter, A. Zeilinger, A.V. Sergienko, and Y. Shih, Phys. Rev. Lett. **75**, 4337 (1995).

[7] D. Bouwmeester, Jian-Wei Pan, K. Mattle, M. Eibl, H. Weinfurter, and A. Zeilinger, Nature (London) **390**, 575 (1997); D. Boschi, S. Branca, F. De Martini, L. Hardy, and S. Popescu, Phys. Rev. Lett. **80**, 1121 (1998).

[8] A.V. Sergienko, M. Atatüre, Z. Walton, G. Jaeger, B.E.A. Saleh, and M.C. Teich, Phys. Rev. A **60**, R2622 (1999); T. Jennewein, C. Simon, G. Weihs, H. Weinfurter, and A. Zeilinger, Phys. Rev. Lett. **84**, 4729 (2000).

[9] O. Jedrkciewicz, Y. Jang, P. Di Trapani, E. Brambilla, A. Gatti, and L.A. Lugiato (unpublished).

[10] R. Zambrini, A. Gatti, M. San Miguel, and L.A. Lugiato, Phys. Rev. A (to be published).

[11] A. Lamas-Linares, J.C. Howell, and D. Bowmeester, Nature (London) **412**, 887 (2001).

[12] M.I. Kolobov, Rev. Mod. Phys. **71**, 1539 (1999).

[13] E. Brambilla, A. Gatti, and L.A. Lugiato (unpublished); e-print quant-ph/0306116.

[14] Pierre Scotto and Maxi San Miguel, Phys. Rev. A **65**, 043811 (2002).

[15] Note that the presence of the crystal length parameter l_c is not strictly necessary in Eq. (4), but it has been introduced with the purpose of defining a dimensionless phase-mismatch parameter.

[16] K. Katz, IEEE J. Quantum Electron. **22**, 1013 (1986).

[17] N. Boeuf, D. Branning, I. Chaperot, E. Dauler, S. Guerin, G. Jaeger, A. Muller, and A. Migdall, Opt. Eng. **39**, 1016 (2000).

[18] See http://physics.nist.gov/Divisions/Dv844/facilities/cprad.html

[19] M. Born and E. Wolf, *Principles of Optics* (Pergamon, Oxford, 1975).

[20] Goodman, *Introduction to Fourier Optics*, p. 83 (McGraw-Hill, New York).

[21] E. Brambilla, A. Gatti, and L.A. Lugiato, Eur. Phys. J. D **15**, 127 (2001); A. Gatti, E. Brambilla, L.A. Lugiato, and M.I. Kolobov, Phys. Rev. Lett. **83**, 1763 (1999).

[22] I.V. Sokolov, M.I. Kolobov, and L.A. Lugiato, Phys. Rev. A **60**, 2420 (1999).

[23] Similar calculations are reported in detail in the first reference of Ref. [21], for a type-I crystal and in C. Szwaj, G.-L. Oppo, A. Gatti, and L.A. Lugiato, Eur. Phys. J. D **10**, 433 (2000), for a nondegenerate optical parametric oscillator.

[24] Lu-Ming Duan, G.I. Giedke, J.I. Cirac, and P. Zoller, Phys. Rev. Lett. **84**, 2722 (2000).

[25] J. Rarity (private communication).

[26] B.E.A. Saleh (private communication).

[27] S.M. Barnett and P.M. Radmore, *Methods in Theoretical Quantum Optics* (Clarendon Press, Oxford, 1997).